# High variability of particulate organic carbon export along the North Atlantic GEOTRACES section GA01 as deduced from $^{234}$Th fluxes

Nolwenn Lemaitre[1,2,3,] Frédéric Planchon[2], Hélène Planquette[2], Frank Dehairs[3], Debany Fonseca-Batista[3,4], Arnout Roukaerts[3], Florian Deman[3], Yi Tang[5,6], Clarisse Mariez[2], Géraldine Sarthou[2]

[1]Department of Earth Sciences, Institute of Geochemistry and Petrology, ETH-Zürich, Zürich, Switzerland
[2]Laboratoire des Sciences de l'Environnement Marin (LEMAR), UMR 6539, IUEM, Technopôle Brest Iroise, 29280 Plouzané, France
[3]Vrije Universiteit Brussel, Analytical, Environmental and Geo-Chemistry, Earth System Sciences research group, Brussels, Belgium
[4]Oceanography Department, Dalhousie University, Halifax, Nova Scotia, Canada
[5] Earth and Environmental Sciences, the Graduate Center, City University of New York, New York, USA
[6] School of Earth and Environmental Sciences, Queens College, City University of New York, Flushing, USA

Correspondence to: Nolwenn Lemaitre (nolwenn.lemaitre@erdw.ethz.ch)

**Abstract.** In this study we report particulate organic carbon (POC) export fluxes for different biogeochemical basins of the North Atlantic as part of the GEOTRACES GA01 expedition (GEOVIDE, May-June 2014). Surface POC export fluxes were deduced by combining export fluxes of total $^{234}$Th with the POC to $^{234}$Th ratio of sinking particles at the depth of export. Particles were collected in two size classes (> 53 µm and 1-53 µm) using *in-situ* pumps and the large size fraction was considered as representative of sinking material. Surface POC export fluxes revealed latitudinal variations between provinces ranging from 1.4 mmol m$^{-2}$ d$^{-1}$ in the Irminger basin where the bloom was close to its maximum, to 12 mmol m$^{-2}$ d$^{-1}$ near the Iberian Margin where the bloom had already declined. In addition to the state of progress of the bloom, variations of the POC export fluxes were also related to the phytoplankton size and community structure. In line with previous studies, the presence of coccolithophorids and diatoms appeared to enhance the POC export flux, while dominance of pico-phytoplankton cells, such as cyanobacteria, resulted in lower fluxes. The POC export to primary production (PP) ratio strongly varied regionally and was generally low (≤ 14 %), except at two stations located near the Iberian margin (35%) and within the Labrador basin (38%), which were characterized by unusual low *in-situ* PP. We thus conclude that the North Atlantic during the GEOVIDE cruise was not as efficient in exporting carbon from the surface, as reported earlier by others. Finally, we also estimated the POC export at 100 m below the surface export depth to investigate the POC transfer efficiencies. This parameter was also highly variable amongst regions, with the highest transfer efficiency at sites where coccolithophorids dominated.

## 1. Introduction

Through the sinking of particulate biogenic material, the biological carbon pump (BCP) plays a major role on the sequestration of carbon-rich particles in the ocean interior. The North Atlantic harbors one of the most productive spring phytoplankton bloom of the world's ocean (Esaias et al., 1986; Longhurst, 2010), generating an important pulse of biogenic sinking particles (Buesseler et al., 1992; Honjo and Manganini, 1993; Le Moigne et al., 2013a),

39   which accounts up to 18% of the global BCP (Sanders et al., 2014). Yet, a substantial range of carbon export

40   efficiencies (1-47%) has been reported by earlier studies at different locations of the North Atlantic (Buesseler et

41   al., 1992; Buesseler and Boyd, 2009; Ceballos-romero et al., 2016; Herndl and Reinthaler, 2013; Lampitt et al.,

42   2008; Moran et al., 2003; Mouw et al., 2016; Thomalla et al., 2008), directly questioning about how carbon export

43   efficiency varies at a trans-Atlantic scale and what are the controlling factors.

44   The international GEOTRACES program aims to measure trace elements and isotopes along full-depth ocean

45   sections through each of the major ocean basins in order to provide maximum scientific rewards on a global scale

46   (GEOTRACES, 2006). The GEOVIDE GA01 section in the high-latitude North Atlantic (15 May - 30 June 2014;

47   R/V Pourquoi Pas?), was a French contribution to this global survey. The studied area crossed five basins

48   differentiated by their distinct biogeochemical and hydrodynamic characteristics: the Iberian basin, the west

49   European basin, the Icelandic basin, the Irminger basin and the Labrador basin (Fig.1).

50   The low nutrient availabilities (surface nitrate and silicate concentrations $< 1$ µmol L$^{-1}$; nutrient analyses according

51   to Aminot and Kérouel, 2007) in the Iberian basin limits the biomass development giving the opportunity to pico-

52   phytoplankton, such as cyanobacteria, to grow (~ 35% of the total Chl-$a$ at Station 13; Tonnard et al., in prep.;

53   pigment analyses according to Ras et al., 2008), a situation which is typical for the North Atlantic subtropical gyre

54   (Moore et al., 2008; Zehr and Ward, 2002). The Iberian basin can also be influenced by a local upwelling, close

55   to the Iberian margin (Costa Goela et al., 2016; Zúñiga et al., 2016; http://marine.copernicus.eu/) and potentially

56   fueling the area with nutrient-rich, but upwelling was not active during GEOVIDE (Shelley et al., 2016).

57   In the subpolar region, in the Irminger and Labrador basins, phytoplankton growth is strongly light-limited

58   seasonally (Riley, 1957) and the key parameter for alleviating these limitations is the progressive shoaling of the

59   mixed layer. There, micro-phytoplankton, such as diatoms, dominate the phytoplankton bloom ($\geq$ 50% of the total

60   Chl-$a$; Tonnard et al., in prep.). Both basins were influenced by strong hydrodynamic features, such as the Irminger

61   gyre, the Eastern Greenland Current (EGC), the Western Greenland Current (WGC), the Labrador Current (LC;

62   Zunino et al., 2017) and the subduction of the Labrador Seawater (LSW) which was particularly intense (1700 m-

63   deep convection) during the winter 2013-2014 (Kieke and Yashayaev, 2015).

64   Between the subtropical and subpolar regions, the west European and Icelandic basins represent a transition zone

65   where nutrients and/or light can limit primary production (Henson et al., 2009). During GEOVIDE, the silicic acid

66   stock was low ($\leq 1$ µmol L$^{-1}$) leading to the growth of nano-phytoplankton, such as haptophytes including

67   coccolithophorids (between 45 and 80% of the total Chl-$a$; Tonnard et al., in prep.). This region is influenced by

68   the Eastern Reykjanes Ridge Current (ERRC) and by the North Atlantic Current (NAC) with the southernmost

69   sub-branch evolving in a cyclonic eddy and the sub-arctic front (SAF). SAF separates cold and fresh waters from

70   the subpolar region and the warm and salty waters from the subtropical region (Zunino et al., 2017).

71   The North Atlantic is thus a heterogeneous basin in terms of nutrient status, phytoplankton communities and

72   hydrodynamic features.

73   This is of a crucial importance as ecosystem structure is thought to play an important role on the BCP. Guidi et al.

74   (2009) suggested that phytoplankton composition explained 68% of the variance in POC flux at 400 m. High

75   export efficiencies are reported in productive regions where diatoms dominate, but the exported material is

76   relatively labile and prone to remineralisation leading to low transfer efficiency and low deep export flux (Guidi

77   et al., 2009). Conversely, in oligotrophic regions, where diatoms are largely absent, primary production is low and

78   mostly regenerated. Consequently, export efficiencies are low but the eventual exported material is likely less

79   prone to dissolution - remineralisation, resulting in high transfer efficiencies (Henson et al., 2012; Lam et al., 2011;
80   Lima et al., 2014; Marsay et al., 2015). Phytoplankton size structure has also been shown to be an important factor
81   in controlling the POC export fluxes. Guidi et al. (2015) highlighted that the exported POC was more refractory
82   and the remineralisation depth was deeper when the fraction of micro-phytoplankton decreased or the fraction of
83   pico-phytoplankton increased.

84   Due to the complex impact of these biogeochemical factors on the POC export and according to the distinct
85   features of each biogeochemical basin, the efficiency of the North Atlantic to transfer POC to the deep ocean
86   deserves more study.

87   In this context, we investigated POC export fluxes derived from the Thorium-234 ($^{234}$Th) approach along a transect
88   in the high-latitude North Atlantic, from the Iberian margin to the sub-arctic Irminger and Labrador Seas. $^{234}$Th, a
89   highly particle reactive element with a short half-life (24.1 d), is widely used to explore particle export over short
90   time events such as phytoplankton blooms (Bhat et al., 1969; Buesseler et al., 1992; Coale and Bruland, 1985;
91   Cochran and Masqué, 2003). A deficit of $^{234}$Th with respect to its radioactive parent $^{238}$U (conservative in seawater)
92   is usually observed in the upper water column where particles sink. In the subsurface waters any excess of $^{234}$Th
93   relative to $^{238}$U, is taken to reflect particle break-up and remineralisation by heterotrophic bacteria and/or
94   zooplankton (Buesseler et al., 2008; Maiti et al., 2010; Savoye et al., 2004). A $^{234}$Th flux can be converted into a
95   POC flux by using the POC:$^{234}$Th ratio of sinking particles at the depth of export (Buesseler et al., 2006).

96   In this study, we discuss carbon export fluxes determined at the base of the deficit zone according to the
97   biogeochemical properties found in each basins, with special emphasis on the stage and intensity of the bloom as
98   well as on the phytoplankton community structure. Using estimates of primary production from shipboard
99   incubations and satellite-derived Chl-*a*, we explore surface export efficiencies at different time scales over the
100   studied area. In addition and using deep carbon export, we investigate POC transfer efficiency in the upper
101   mesopelagic.

102   **2.   Methods**

103   **2.1.   Total $^{234}$Th and $^{238}$U**

104   Total $^{234}$Th activities were determined from 4 L unfiltered seawater samples collected with 12L Niskin bottles.
105   Usually, 17 or 18 depths were sampled between the surface and 1000-1500 m, except at Stations 26 and 77 where
106   only 9 and 15 depths were sampled, respectively (Table S1). Deep samples (between 1000 and 3500 m) were taken
107   for the calibration of the low level beta counting (Rutgers van der Loeff et al., 2006) based on the knowledge that
108   $^{234}$Th and $^{238}$U are generally in secular equilibrium at such depths (in this study, the deep ocean average $^{234}$Th/$^{238}$U
109   ratio = 1.00 ± 0.02; n=15). Seawater samples were processed following the method developed by Pike et al. (2005).
110   Samples were acidified at pH 2 and spiked with a $^{230}$Th yield monitor in order to estimate the $^{234}$Th recovery during
111   the sample processing. After 12 hours of equilibration, pH was increased to 8.5 and $KMnO_4$ and $MnCl_2$ (analytical
112   grade, Merck) were added to form a manganese oxide precipitate. After a further 12 hours of equilibration, samples
113   were filtered on quartz-microfiber discs (QMA, Sartorius, 1 µm nominal porosity, 25 mm diameter). On board,
114   filters were dried overnight, mounted on nylon holders, and covered with Mylar and aluminum foil. The activity
115   of $^{234}$Th on each sample was counted using low level beta counters (RISØ, Denmark). Beta activity counting was
116   continued until a relative standard deviation (RSD) ≤ 2% was reached. At the home-laboratory, residual beta

activity was measured for each sample after a delay of six $^{234}$Th half-lives (~ 6 months) and these residual counts were subtracted from the gross counts obtained on-board. All samples were then processed for Th recovery using $^{229}$Th as a second yield tracer. To do so, filters were dismounted from the nylon holders and transferred to clean 30 mL teflon vials (Savillex). All samples were spiked with $^{229}$Th, dissolved in a mix of 8M HNO$_3$/1M H$_2$O$_2$ (suprapur grade, Merck), heated overnight and filtered through Acrodisc® syringe filters (Pall, Nylon membrane, nominal porosity=0.2 µm, diameter=25 mm). Part of the filtrate was pre-concentrated by evaporation and the residue diluted in 1.4 M HNO$_3$ (suprapur grade, Merck). $^{230}$Th and $^{229}$Th concentrations were measured by sector field inductively coupled plasma mass spectrometry (SF-ICP-MS, Element 2, Thermo Scientific) in low resolution mode. Each sample was analyzed 3 times and the precision of the $^{230}$Th:$^{229}$Th ratios averaged 1.2% (RSD), which is within the range indicated by Pike et al. (2005). The total $^{234}$Th recovery, involving all the steps described above, was 91 ± 14% (n=200). Uncertainty of total $^{234}$Th activity, estimated from error propagation, was between 0.04 and 0.10 dpm L$^{-1}$.

The $^{238}$U activity was deduced from salinity using the Eq. 1, given by Owens et al. (2011):

$$^{238}U = 0.0786 \times S - 0.315 \qquad (1)$$

where $^{238}$U is the $^{238}$U activity in dpm L$^{-1}$ and S is salinity.

## 2.2. Particulate $^{234}$Th and POC sampling and analysis

Suspended particles were collected using *in-situ* large-volume filtration (100-1600 L) systems (Challenger Oceanics and McLane pumps; ISP hereafter for "*in-situ* pumps") through paired 142 mm-diameter filters: a 53 µm mesh nylon screen (SEFAR-PETEX®; polyester) and a 1 µm pore size quartz-microfiber filter (QMA, Sartorius), respectively. The small size fraction (1-53 µm) is referred to hereafter as SSF and the large size fraction (> 53 µm) as LSF. Prior to the cruise, filters were cleaned as follows: PETEX screens were soaked in 0.6 M HCl (Normapur, Merck), rinsed with Milli-Q water, dried at ambient temperature in a laminar flow hood, and stored in clean plastic bags; QMA filters were pre-combusted at 450 °C for 4 h and stored in aluminum foils until use. ISP were deployed between 15 and 800 m on a stainless steel cable and the pumping time was approximatively 2-3 h (Table S2).

After collection, filters were processed on board. The 142 mm PETEX screen was cut into quarters using a clean scalpel and two quarters were processed in this study. Particles were rinsed-off from the PETEX screen using 0.45 µm filtered seawater under a laminar flow hood. For one quarter of the PETEX screen, the rinsed-off particles were re-filtered on a silver filter (SterliTech, porosity=0.45 µm, diameter=25 mm) and for the other quarter on a GF/F filter (Whatman®, porosity=0.7 µm, diameter=25 mm). The QMA filters were sub-sampled with a perspex punch of 25 mm diameter. Silver, GF/F and QMA filters were dried overnight and prepared for beta counting (see section 2.1). After counting the residual beta activity (~ 6 months later), samples were prepared for POC, particulate nitrogen (PN) analyses along with their $\delta^{13}$C and $\delta^{15}$N isotopic compositions (here we present only POC data). Filters were dismounted from filter holders and fumed with HCl vapor overnight inside a glass desiccator to remove the carbonate phase. Samples were dried, packed in precombusted (450 °C overnight) silver cups, and analyzed with an elemental analyzer – isotope ratio mass spectrometer (EA-IRMS, Delta V Plus, Thermo Scientific). Acetanilide standards were used for the calibration. The detection limits and C blanks were respectively 0.63 and 0.80 µmol for Ag filters (n=11) and were 0.49 and 1.52 µmol for QMA filters (n=13).

154 The POC concentrations and $^{234}$Th activities compared well between silver and GF/F filter types pointing to the
155 rather homogenous distribution of the particles on the Petex screen ($^{234}$Th$_{GFF}$ = 0.63 × $^{234}$Th$_{silver}$ + 0.01 with r$^2$=0.88,
156 p-value<0.01 and n=58; and POC$_{GFF}$= 0.86 POC$_{silver}$ + 0.08 with r$^2$=0.90, p-value<0.01 and n=58; Fig. S1),
157 although concentrations from GF/F filters were systematically lower than those from silver filters, most likely
158 because of the different pore size filter (0.7 µm for GF/F filter vs 0.45 µm for silver filter).

## 2.3. Export fluxes of $^{234}$Th

160 Thorium-234 activity in surface waters can be described using a simple mass balance equation (Savoye et al.,
161 2006), which accounts for production from $^{238}$U decay, $^{234}$Th decay, sinking flux and transport as follow:

$$\frac{dA_{Th}}{dt} = \lambda A_U - \lambda A_{Th} - P + V \qquad (2)$$

163 where $A_{Th}$ is the activity of total $^{234}$Th in dpm L$^{-1}$; $A_U$ is the salinity-derived activity of $^{238}$U in dpm L$^{-1}$, $\lambda$ is the
164 $^{234}$Th decay constant (0.0288 d$^{-1}$); P is the net removal of $^{234}$Th on sinking particles in dpm L$^{-1}$ d$^{-1}$; V is the sum of
165 the advective and diffusive fluxes in dpm L$^{-1}$ d$^{-1}$.

166 Assuming steady state (constant total $^{234}$Th activity with time) and neglecting the physical term V (Buesseler et
167 al., 1992), the net export flux of particulate $^{234}$Th can be determined using the following equation:

$$P = \lambda \int_0^z (A_U - A_{Th})dz \qquad (3)$$

169 where P is the integrated flux of $^{234}$Th from the surface to the depth z in dpm m$^{-2}$ d$^{-1}$. Eq. 3 has been solved for z
170 taken as the depth (Eq) at the base of the $^{234}$Th deficit zone (Eq = depth where $^{234}$Th activity is back to secular
171 equilibrium with $^{238}$U) as well as for z representing the base of the primary production zone (PPZ), i.e. the depth
172 where *in-situ* fluorescence was only 10% of its maximum value (Owens et al., 2014). The Eq depth matched
173 relatively well with the PPZ depth, and on average, difference between both was only 16 m, with the largest
174 difference (~ 60 m) at Stations 1, 32 and 51 (Fig. 2). Considering that there can be export (or remineralisation)
175 below or above the PPZ depth, only the export fluxes at the Eq depth will be discussed as they represent the fully-
176 integrated depletion of $^{234}$Th in the upper waters and thus the maximal export. The validity of the assumptions
177 used for solving Eq. 3 is discussed in Section 4.1.

178 In Section 4.1.2, we attempt to calculate the $^{234}$Th fluxes at the Eq depth by using a non-steady state (NSS) model
179 (Savoye et al., 2006), which can be described as follows:

$$P = \lambda \left[ \frac{A_U \left(1 - e^{-\lambda \Delta t}\right) + A_{Th1} e^{-\lambda \Delta t} - A_{Th2}}{1 - e^{-\lambda \Delta t}} \right] \qquad (4)$$

181 where $\Delta t$ is the time interval between two visits of a single station; $A_{Th1}$ and $A_{Th2}$ are the $^{234}$Th activities at the first
182 and second visits, respectively. Without time series data, the calculation should not be performed sensu stricto
183 (Buesseler et al., 1992; Savoye et al., 2006) but we chose to set the initial conditions for each station, as done by
184 Rutgers van der Loeff et al. (2011) in the South Atlantic. Satellite-derived PP data were used to estimate the starting
185 date of the bloom (i.e., when there is a PP increase of 30% above the winter value) and $^{234}$Th was assumed to be
186 in equilibrium with $^{238}$U at this time point. The time interval ($\Delta t$) for the calculations stretched from the bloom
187 start until the sampling date. All physical terms were considered negligible.

To estimate the intensity of shallow remineralization, export flux was also calculated for the Eq+100 m depth horizon. In case of any $^{234}$Th excess relative to $^{238}$U (i.e., $^{234}$Th/$^{238}$U ratio > 1) below the Eq depth due to remineralisation, export fluxes integrated until Eq+100 m will be less than when integrated until Eq. Following Black et al. (2017) the reduction of the $^{234}$Th flux, R100, is expressed as:

$$R100 = P_{Eq} - P_{Eq+100} \qquad (5)$$

where R100 is the flux reduction in dpm m$^{-2}$ d$^{-1}$ and P is the $^{234}$Th export flux estimated at Eq or Eq+100.

### 2.4. Scavenging fluxes of $^{234}$Th

To estimate the transfer rate of $^{234}$Th from the dissolved to the particulate form, i.e., the scavenging flux of $^{234}$Th (Coale and Bruland, 1985), we deduced the dissolved $^{234}$Th activities by subtracting the particulate (SSF+LSF) from the total $^{234}$Th activities, keeping in mind, though, that the sampling method for the total and particulate phases differed. Because the sampling resolution was different, total $^{234}$Th data were averaged at the sampling depth of particulate $^{234}$Th.

The mass balance equation for dissolved $^{234}$Th can be written as follows:

$$\frac{dA_{Thd}}{dt} = \lambda A_U - \lambda A_{Thd} - J + V \qquad (6)$$

where $A_{Thd}$ is the activity of dissolved $^{234}$Th in dpm L$^{-1}$; $A_U$ and $\lambda$ are defined in Eq. 2; J is the net removal flux from the dissolved to the particulate form (scavenging flux) in dpm L$^{-1}$ d$^{-1}$; and V is the sum of the advective and diffusive fluxes in dpm L$^{-1}$ d$^{-1}$.

Using again the steady state assumption (dissolved $^{234}$Th activities remain constant over time) and ignoring the physical terms (V), Eq. 6 becomes:

$$J = \lambda \int_0^z (A_U - A_{Thd}) dz \qquad (7)$$

where J in dpm m$^{-2}$ d$^{-1}$ is the net flux of scavenging integrated to the depth z. In our case, the calculation was performed at the Eq depth for comparison with the $^{234}$Th export flux (P in Eq. 3).

The comparison between the export flux (P) and scavenging flux (J) in terms of P/J ratio (export ratio) offers a valuable metric for estimating the export efficiency of $^{234}$Th. A low P/J ratio (< 0.5) indicates that the removal of dissolved $^{234}$Th is controlled by sorption onto suspended particles rather than export. Conversely, a high P/J ratio (> 0.5) indicates that $^{234}$Th is preferentially exported rather than adsorbed and is thus efficiently removed from the upper waters.

### 2.5. POC:$^{234}$Th ratios and POC export fluxes

We estimated POC export fluxes by multiplying the $^{234}$Th export flux with the POC:$^{234}$Th ratio, both determined at the Eq depth. A power law fit was used to determine the POC:$^{234}$Th ratios at Eq (Fig. 3). Errors of the POC:$^{234}$Th ratios extrapolated at the Eq depth are deduced from the power law fit, using a root sum squared method. This error is much larger than analytical errors of both POC concentrations and particulate $^{234}$Th activities. POC fluxes

220 were determined by using the POC:[234]Th ratios of the LSF (> 53 µm) as well as the SSF (1-53 µm) samples, and
221 both estimations were compared (Table 2).

222 The POC fluxes were between 1.1 to 1.5 fold higher when using the SSF POC:[234]Th ratio, except at stations 1, 26
223 and 64. However, when considering the uncertainties, POC fluxes based on SSF and LSF POC:[234]Th ratios were
224 not significantly different, and as we did not have the possibility to compare the POC:[234]Th ratios with those from
225 sediment traps, we cannot affirm that the small particles participated to the export. As large and rapidly sinking
226 particles usually drive most of the export (Lampitt et al., 2001; Villa-Alfageme et al., 2016), most of the studies
227 dedicated to POC export fluxes in the North Atlantic used the POC:[234]Th ratios from the LSF (see Le Moigne et
228 al., 2013b; Puigcorbé et al., 2017). Therefore, only the POC fluxes determined with the POC:[234]Th ratios from the
229 LSF will be discussed (Table 3).

### 2.6. In-situ primary production

231 In order to determine the *in-situ* daily PP, stable isotope incubations were conducted using seawater collected at
232 different euphotic zone depths selected using photosynthetically active radiation (PAR) profiles, as described in
233 more detail in Fonseca-Batista et al. (2018). At each station, seawater was sampled from 3 to 6 depths (from 54 to
234 0.2% of surface PAR) and incubated on deck with a $H^{13}CO_3^-$ enriched substrate. After 24 h, incubated samples
235 were filtered through microglass fiber filters (MGF, 0.7 µm porosity, Sartorius). At the home-laboratory, POC
236 concentrations and isotopic composition were analyzed by EA-IRMS and uptake rates were deduced following the
237 Hama et al. (1983) method. Daily PP was then estimated by integrating the uptake rates from the surface down to
238 0.2% of surface PAR, which was located between 48 and 116 m depending on the station. The 0.2% of surface
239 PAR depth was roughly corresponding to the Eq depth (median difference between both depths: $20 \pm 13$ m)
240 although, a 42 m difference was observed at Station 1. Note that at Station 51, PP was determined 24 h after the
241 sampling of the total [234]Th, particulate [234]Th and POC.

### 2.7. Satellite primary production

243 PP was also obtained from satellite data products with a 9 km spatial resolution and 8-day temporal resolution,
244 available from the Ocean Productivity website at Oregon State University
245 (http://www.science.oregonstate.edu/ocean.productivity/) and obtained from MODIS and SeaWiFS satellites.
246 Three different models can be used to obtain satellite-derived PP: the standard Vertically Generalized Production
247 Model (VGPM; (Behrenfeld and Falkowski, 1997), the Eppley-VGPM (Eppley, 1972) and the Carbon-Based
248 Production Model (CbPM; Behrenfeld et al., 2005; Westberry et al., 2008). Among the model outputs, VGPM
249 derived PP (VGPM-PP) are closest to the *in-situ* PP measurements during our study (Fig. 4). Therefore, VGPM-
250 PP is used in later discussion.

251 VGPM-PP data were averaged over $5 \times 5$ pixel boxes corresponding to a surface area of 2025 km² (45 km×45 km)
252 centered on the different sampling stations and the VGPM-PP was averaged for the week (8 days), the month (32
253 days) and the whole productive period prior to the sampling date. The whole productive period is the period
254 between the bloom start (defined by a PP increase of 30% above the winter value) and the sampling date (Fig. 5).
255 Differences between the different VGPM-PP estimates were smaller than a factor of 1.5.

## 3. Results

### 3.1. The Iberian basin (Stations 1 and 13)

Stations 1 and 13 were sampled 10 to 12 weeks after the start of the bloom (Fig. 4). At these stations, PP increased very early in the year (early to mid-March) and collapsed rapidly (end of March to mid-April). Within the Iberian basin, low *in-situ* PP were determined (Table 3), with one of the lowest values measured at Station 1 (33 mmol m$^{-2}$ d$^{-1}$) and a moderate PP at Station 13 (79 mmol m$^{-2}$ d$^{-1}$; Fonseca-Batista et al., 2018; this issue).

In line with low *in-situ* PP, low POC concentrations and particulate $^{234}$Th activities were determined in the Iberian basin (Table S2). POC:$^{234}$Th ratios were low in both size fractions at Station 13, while Station 1 had high ratios, reaching 31 µmol dpm$^{-1}$ in surface for the LSF (Fig. 3). Similarly, Station 13 had the lowest LSF POC:$^{234}$Th ratio extrapolated at Eq whereas Station 1 had one of the highest ratios (Table 3).

The $^{234}$Th/$^{238}$U ratios were in the median of the range observed along the transect and reached minima of 0.68 and 0.70 in the upper 40 m at Stations 1 and 13, respectively (Fig. 2). Interestingly, these two stations vary also in their total particulate $^{234}$Th (sum of the SFF and LSF) over total $^{234}$Th ratios with only 9% of the $^{234}$Th in the particulate phase at Station 1 and a ratio of 28% at Station 13 (in the median of those observed elsewhere along the transect). At both stations, the $^{234}$Th export fluxes at the Eq depth were slightly higher than the median value observed along the transect (1135 dpm m$^{-2}$ d$^{-1}$, n=11), reaching 1264 and 1418 dpm m$^{-2}$ d$^{-1}$ at Stations 1 and 13, respectively (Table 1). Compared to Station 1, the $^{234}$Th scavenging flux was ~ 2 fold higher at Station 13 (1509 and 2898 dpm m$^{-2}$ d$^{-1}$, respectively; Table 1). Consequently, the export ratio (P/J) was higher at Station 1, reaching 0.84, compared to Station 13 (P/J ratio=0.49; Fig. 6). This indicates a balanced situation between P and J fluxes at Station 13 and a more efficient export of $^{234}$Th by sinking particles at Station 1.

Below Eq, significant excesses of $^{234}$Th relative to $^{238}$U (i.e., $^{234}$Th/$^{238}$U ratio > 1.1) were observed at both stations, indicating particle degradation (Fig. 2). However, significant shallow remineralisation was only observed at Station 13 for which the R100 value was above uncertainty, reaching 410 ± 218 dpm m$^{-2}$ d$^{-1}$ (Table 1). This represents a flux reduction of 30% relative to the surface export flux.

Similarly, POC export fluxes varied between both stations with the highest (albeit with a strong associated error; 12 mmol m$^{-2}$ d$^{-1}$ at Station 1) and one of the lowest (2.2 mmol m$^{-2}$ d$^{-1}$ at Station 13) fluxes along the transect observed within this basin.

### 3.2. The west European basin (Stations 21 and 26)

During 2014, the west European basin was the most productive with the highest PP peak observed at Station 21 (403 mmol m$^{-2}$ d$^{-1}$), 13 days before the sampling. At Station 26, the sampling took place during a secondary PP increase (Fig. 4 and 5). Altogether, sampling coincided with the bloom development in this basin, with *in-situ* PP reaching 135 and 174 mmol m$^{-2}$ d$^{-1}$ at Stations 21 and 26, respectively (Table 3).

Along with high PP, relatively high surface POC concentrations and particulate $^{234}$Th activities were measured averaging 3.7 µmol L$^{-1}$ and 0.2 dpm L$^{-1}$ for the LSF and, 5.4 µmol L$^{-1}$ and 0.5 dpm L$^{-1}$ for the SSF (Table S2). For both size fractions, POC:$^{234}$Th ratios were high in the upper water column, reaching a maximum of 30 µmol dpm$^{-1}$ for the LSF in surface waters at Station 21 (Fig. 3). At the Eq depth, the POC:$^{234}$Th ratios for the LSF were in the median of those determined along the transect (4.4 µmol dpm$^{-1}$, n=11) with nevertheless a lower ratio at Station 21 (2.6 µmol dpm$^{-1}$; Table 3).

294     The lowest $^{234}$Th/$^{238}$U ratios were observed in the surface waters of the west European basin reaching minima of

295     0.57 and 0.77 at Stations 21 and 26, respectively (Fig. 2). Moreover, these low ratios were observed deeper in the

296     water column compared to the other basins. The integration of the $^{234}$Th deficit from the surface to the Eq depth

297     led thus to high $^{234}$Th export fluxes at both stations. The $^{234}$Th export flux at Station 21 was one of the highest

298     observed along the transect, reaching 1873 dpm m$^{-2}$ d$^{-1}$ (Table 1). The $^{234}$Th scavenging fluxes were also among

299     the highest observed along the transect, reaching 3917 and 2839 dpm m$^{-2}$ d$^{-1}$ at Stations 21 and 26, respectively

300     (Table 1). The resulting export ratio (P/J) was close to 0.5 for both stations, indicating a balanced situation between

301     export and scavenging fluxes.

302     Excess of $^{234}$Th relative to $^{238}$U below Eq, was observed at both stations, with $^{234}$Th/$^{238}$U ratios reaching 1.14 at

303     300 m for Station 21 (Fig. 2; Table S1). Consequently, the R100 value at this station was significantly positive

304     (360 ± 255 dpm m$^{-2}$ d$^{-1}$; Table 1), representing a 20% $^{234}$Th flux reduction.

305     Relatively high POC export fluxes at Eq were observed in the west European basin, reaching respectively 4.8 and

306     7.9 mmol m$^{-2}$ d$^{-1}$ at Stations 21 and 26. For the same area, other studies reported similar POC export fluxes during

307     May (Thomalla et al., 2008), and July-August (Lampitt et al., 2008; Le Moigne et al., 2013). However, Buesseler

308     et al. (1992) report much higher POC fluxes (up to 41 mmol m$^{-2}$ d$^{-1}$) for April-May during the North Atlantic

309     Bloom Experiment, highlighting an important temporal variability of POC export flux in this basin (Fig. 7).

310     **3.3. The Icelandic basin (Stations 32 and 38)**

311     In general, the different fluxes in the Icelandic basin presented similar characteristics to those in the west European

312     basin.

313     The bloom period started in May, one month before the sampling and the bloom maximum occurred after the

314     cruise (Fig. 4). Nevertheless, the basin was highly productive at Station 32 with *in-situ* PP reaching 105 mmol m$^{-2}$

315     d$^{-1}$ and was relatively productive at Station 38 (68 mmol m$^{-2}$ d$^{-1}$; Table 3 and Fig. 4 and 5).

316     POC concentrations and particulate $^{234}$Th activities were relatively high, but unlike for the west European basin

317     the highest concentrations and activities were found in the SSF, reaching 5.8 µmol L$^{-1}$ and 0.4 dpm L$^{-1}$, respectively

318     at Station 32 (Table S2). For surface waters of both stations, POC:$^{234}$Th ratios in the SSF exceeded those in the

319     LSF (Fig. 3) but ratios were similar between the two size fractions at Eq depth (difference less than a factor of

320     1.1). The ratios extrapolated to Eq for the LSF were 3.6 and 4.2 µmol dpm$^{-1}$ at Stations 32 and 38, respectively

321     and were in the median of the range along the transect (Table 3).

322     As for the west European basin, $^{234}$Th/$^{238}$U ratios were low with station 38 having the lowest value for the whole

323     transect (0.50 in the surface; Fig. 2). Low ratios were also observed deeper in the water column and the combination

324     yielded the highest $^{234}$Th export fluxes at Eq, reaching 2282 ± 119 dpm m$^{-2}$ d$^{-1}$ at Station 32 (Table 1). While the

325     $^{234}$Th scavenging flux was high at Station 32, reaching 3690 dpm m$^{-2}$ d$^{-1}$, it was much lower at Station 38 (1495

326     dpm m$^{-2}$ d$^{-1}$; Table 1). The export ratios (P/J) slightly exceeded the median value along the transect, reaching 0.62

327     and 0.76 at Stations 32 and 38, respectively. Despite similarities with the west European basin, the Icelandic basin

328     appeared more efficient to export $^{234}$Th by sinking particles.

329     Below the Eq depth, there was no significant excess of $^{234}$Th relative to $^{238}$U, resulting in R100 values being close

330     or below uncertainty and indicating absence of significant shallow remineralisation.

331     One of the highest POC export fluxes along the transect was determined at Station 32, reaching 8.3 mmol m$^{-2}$ d$^{-1}$

332     while the POC flux at Station 38 was lower (4.8 mmol m$^{-2}$ d$^{-1}$). Such POC export fluxes are lower than most values

333  reported in earlier studies, ranging from 6 to up to 52 mmol m$^{-2}$ d$^{-1}$ although Martin et al. (2011) reported a very

334  low value of 0.8 mmol m$^{-2}$ d$^{-1}$. (Ceballos-romero et al., 2016; Giering et al., 2016; Martin et al., 2011; Sanders et

335  al., 2010; Fig. 7).

### 3.4.  The Irminger basin (Stations 44 and 51)

337  The ship crossed the Irminger basin one month after the beginning of the bloom and sampling occurred just 1 week

338  (Station 44) to 3 weeks (Station 51) after the peak of the bloom (Fig. 4). At sampling time, the *in-situ* PP was

339  amongst the highest observed along the whole section, reaching respectively 137 and 166 mmol m$^{-2}$ d$^{-1}$ at Stations

340  44 and 51. Such high values, in line with the satellite data, suggest that the bloom was still ongoing when visiting

341  these two stations (Table 3 and Fig. 4 and 5).

342  POC concentrations and particulate $^{234}$Th activities were overall highest at these two stations, reaching 17 µmol L$^{-1}$

343  $^{1}$ and 1.2 dpm L$^{-1}$ for the SSF and 4.0 µmol L$^{-1}$ and 0.5 dpm L$^{-1}$ for the LSF at Station 44, respectively (Table S2).

344  POC:$^{234}$Th ratios were moderate for both size fractions, reaching 14 µmol dpm$^{-1}$ for the SSF at Station 44 and 12

345  µmol dpm$^{-1}$ at Station 51 in the surface waters (Fig. 3). At the Eq depth, the extrapolated POC:$^{234}$Th ratios were

346  similar between both size fractions at Station 51 but were 1.7 fold higher in the SSF at Station 44. The POC:$^{234}$Th

347  ratio at Eq in the LSF at Station 44 fitted the median of the ranges determined along the transect, while the ratio at

348  Station 51 was relatively lower (2.9 µmol dpm$^{-1}$, Table 3).

349  The $^{234}$Th/$^{238}$U ratios in the surface waters were higher than at other stations, reaching minima of 0.79 and 0.78 at

350  Stations 44 and 51, respectively. These low $^{234}$Th deficits were also restricted to the upper layer, especially at

351  Station 44 where the Eq depth was 40 m (Fig. 2).The particulate $^{234}$Th (sum of the SFF and LSF) contribution to

352  total $^{234}$Th ratios varied widely, from 27% at Station 51 (in the median of those observed elsewhere along the

353  transect) to 94% at Station 44. The extremely high fraction of particulate $^{234}$Th at Station 44 reflects an important

354  particle concentration in surface waters. On the other hand, this high particulate fraction in the upper layer did not

355  induce a high export flux, since Station 44 had the lowest $^{234}$Th export flux (321 ± 66 dpm m$^{-2}$ d$^{-1}$; Table 1) of all

356  stations. As a result, scavenging fluxes were much higher in this basin, reaching respectively 1802 and 2189 dpm

357  m$^{-2}$ d$^{-1}$ at Stations 44 and 51. This leads to very low P/J ratios in the Irminger basin (as low as 0.2 at Station 44),

358  suggesting that export of $^{234}$Th is particularly inefficient in this basin, in agreement with the low export flux and

359  the high particulate fraction in the upper layer.

360  Below the Eq depth, there was no significant excess of $^{234}$Th relative to $^{238}$U, reflecting no evidence for significant

361  shallow remineralisation, with R100 values being either negative or below uncertainty.

362  The Irminger basin was characterized by low POC export fluxes (1.4 and 2.7 mmol m$^{-2}$ d$^{-1}$ at Stations 44 and 51,

363  respectively). In the literature, a relatively large range of POC export fluxes has been reported for this basin.

364  Puigcorbé et al. (2017) observed POC export fluxes ranging from 1.5 to 43 mmol m$^{-2}$ d$^{-1}$. Ceballos-Romero et al.

365  (2016) also determined much higher POC fluxes compared to those observed in the present study, with differences

366  reaching factors of 27 and 19 for the month before and after our sampling, respectively (Fig. 7).

### 3.5.  The Labrador basin (Stations 64, 69 and 77)

368  Stations of the Labrador basin were sampled approximatively one month after the beginning of the bloom. Station

369  64 was sampled just after a second peak of the bloom while Stations 69 and 77 were sampled one week after this

370  peak (Fig. 4). At sampling time, the *in-situ* PP was low in the Labrador basin, ranging from 27 to 80 mmol m$^{-2}$ d$^{-}$

371  [1] at Stations 69 and 77, respectively (Table 3). In agreement with the satellite data shown in Fig. 4, this indicates

372  that the decline of the bloom was ongoing in the Labrador basin.

373  POC concentrations and particulate $^{234}$Th activities were moderate to low, except at Station 77 where values were

374  higher in the surface, reaching 11 µmol L$^{-1}$ and 0.45 dpm L$^{-1}$ for the SSF, and, 3.0 µmol L$^{-1}$ and 0.20 dpm L$^{-1}$ for

375  the LSF, respectively. Moderate POC:$^{234}$Th ratios were observed in both size fractions, except in the upper layer

376  at station 77 where SSF POC:$^{234}$Th ratios were high (Fig. 3). At the Eq depth, POC:$^{234}$Th ratios were similar in the

377  two size fractions and reached 9.2, 14 and 8.8 µmol dpm$^{-1}$ at Stations 64, 69 and 77, respectively. Interestingly,

378  these ratios are higher than the median ratio determined along the transect.

379  The surface $^{234}$Th/$^{238}$U ratios were in the median of those observed along the transect (0.74 ± 0.06, n=8) with

380  minima of 0.78, 0.66 and 0.73 at Stations 64, 69 and 77, respectively. These $^{234}$Th deficits were nevertheless

381  observed in a relatively shallow layer (Eq depths between 40 and 80 m in this basin; Fig. 2). Stations 64 and 69

382  were also characterized by a low particulate $^{234}$Th activity (combined LSF and SSF) accounting for 10 and 15%

383  of the total $^{234}$Th activity in agreement with relatively low POC concentrations observed at these stations. The

384  $^{234}$Th export flux at Station 64 was slightly greater than those of Stations 69 and 77 but, in general, the $^{234}$Th export

385  fluxes of the Labrador basin were moderate, averaging 758 dpm m$^{-2}$ d$^{-1}$ (Table 1). $^{234}$Th scavenging fluxes were

386  also generally low in the Labrador basin, but with again, a slightly lower scavenging flux at Station 64 (Table 1).

387  A higher export ratio was thus estimated at Station 64 (P/J ratio = 0.75), suggesting a more efficient export close

388  to the Greenland margin compared to Stations 69 and 77 (Fig. 6).

389  Below Eq, there was a significant excess of $^{234}$Th relative to $^{238}$U at Stations 69 and 77, reaching respectively 1.08

390  and 1.11. Evidence for shallow remineralisation was also clear from the R100 values exceeding uncertainties

391  (Station 69, R100=401 ± 159 dpm m$^{-2}$ d$^{-1}$ and Station 77, R100=252 ± 165 dpm m$^{-2}$ d$^{-1}$, Table 1). The flux

392  reductions due to remineralisation below Eq were 50 and 40% of the fluxes at Eq, respectively.

393  High POC exports were observed within the Labrador basin and in particular at Station 69 where POC export flux

394  reached 10 mmol m$^{-2}$ d$^{-1}$. As for the Irminger basin, Puigcorbé et al. (2017) determined a low POC export (0.7

395  mmol m$^{-2}$ d$^{-1}$) in May, one month before our sampling period, while Moran et al. (2003) observed higher fluxes

396  reaching 47 mmol m$^{-2}$ d$^{-1}$ in July, one month after our sampling period (Fig. 7).

397  **4.  Discussion**

398  In the following section, we first discuss the potential impact of the physics and the non-steady state conditions on

399  the $^{234}$Th export flux estimations. Then, temporal and regional variations of the carbon export fluxes are discussed

400  with respect to the intensity and stage of the bloom, the phytoplankton size structure and the phytoplankton

401  community. Finally, we examine carbon export and transfer efficiencies along the transect.

402  **4.1.  Validity of the export estimations**

403  4.1.1. $\underline{^{234}\text{Th export fluxes under the potential influence of physical conditions}}$

404  The GEOVIDE section sampled a diversity of dynamic regimes (Zunino et al., 2017) including continental margins

405  affected by strong zonal surface currents (LC, WGC and EGC; Mercier et al., 2015; Reverdin et al., 2003), local

406  and seasonal upwelling (close to the Iberian Margin), as well as deep convection zone in the Labrador Sea. In such

407  conditions, Eq. 3, which assumes negligible lateral and vertical advective and diffusive fluxes, may not always be

408     appropriate (Savoye et al., 2006). Whenever possible, we explore quantitatively or qualitatively, the potential

409     errors arising from neglecting physical transport in our calculation.

410     Lateral processes associated with high velocity currents and intense mesoscale activity are known to affect the

411     [234]Th distribution (Benitez-Nelson et al., 2000; Resplandy et al., 2012; Roca-Marti et al., 2016b; Savoye et al.,

412     2006). In our case, this may concern several stations located at or close to margins such as Stations 51 and 64,

413     which were respectively subject to the powerful East and West Greenland Currents at the Greenland Margin,

414     Station 77 under the influence of the LC on the Newfoundland Margin and Station 1 under influence of the Portugal

415     Current at the Iberian Margin (Fig. 1). However, the impact of lateral advection cannot be quantified from our

416     dataset, as the possible horizontal gradients of [234]Th cannot be resolved at sufficient resolution. As an alternative,

417     we compare stations close to each other such as Stations 44 and 51, both located in the Irminger Basin where

418     surface currents are strong. The Irminger basin in spring is a really patchy and dynamic area (Ceballos-romero et

419     al., 2016; Le Moigne et al., 2012; Puigcorbé et al., 2017) but the relatively high variability of the [234]Th fluxes

420     found at these two stations (321 and 922 dpm m$^{-2}$ d$^{-1}$, respectively) may also indicate a potential influence of lateral

421     advection. The higher export flux at Station 51 could reflect an input of [234]Th depleted waters originating from the

422     Arctic and/or the Greenland shelf. However, Arctic (Cai et al., 2010; Roca-Marti et al., 2016a) and Greenland shelf

423     waters (Station 53, see Table S1) reveal very limited depletions of [234]Th relative to [238]U. Thus, it is reasonable to

424     consider that the [234]Th deficit at Station 51 was essentially driven by vertical rather than horizontal processes.

425     Hydrodynamic processes could also impact open ocean sites, such as stations within the west European and

426     Icelandic basins (Stations 26 and 32) which are subjected to mesoscale activity. An inverse modeling study carried

427     out for the Porcupine Abyssal Plain located in the same region, suggests that the vertical transport of [234]Th

428     associated with small-scale structures could represent up to 20% of the estimated vertical export flux (Resplandy

429     et al., 2012). This error is larger than our analytical uncertainty and should be kept in mind when considering the

430     export flux data in this area.

431     In upwelling systems, the contribution of vertical advection on the [234]Th distribution has been shown to be

432     important (Buesseler, 1998; Buesseler et al., 1995). Near the Portuguese coast, the intensity of the upwelling is

433     seasonally dependent (Costa Goela et al., 2016; Zúñiga et al., 2016) and was rather inactive at the time of the

434     GEOVIDE cruise (http://marine.copernicus.eu/). Therefore, the input of [234]Th-rich deep waters to the surface is

435     likely to be limited, as already observed in the northern Iberian margin in early summer (Hall et al., 2000).

436     Downwelling systems, such as the intense convection that occurred in the Labrador basin during the winter prior

437     to our sampling (Kieke and Yashayaev, 2015), are also likely to impact the [234]Th distribution. However, a strong

438     vertical advection would homogenize the [234]Th activities in the water column, which is not the case during our

439     study (Fig. 2). Moreover, this convection ended more than two months before our sampling, a time lag that largely

440     exceeds the [234]Th half-life thereby erasing any potential impact on the [234]Th signal. Therefore, the influence of

441     vertical advection on [234]Th export fluxes was neglected.

442     Finally, the contribution of the vertical diffusion was estimated using the vertical gradients of total [234]Th activity

443     in upper waters and a Kz value ranging between 10$^{-4}$ and 10$^{-5}$ m$^2$ s$^{-1}$, as observed in the upper 1000 m between

444     Portugal and Greenland along the OVIDE transect (Ferron et al., 2014). The highest vertical diffusive flux was

445     determined at Station 69 and reached 181 dpm m$^{-2}$ d$^{-1}$, which is in the range of the [234]Th flux uncertainties.

446     Therefore, the impact of the vertical diffusion has not been considered further.

447  In conclusion, hydrodynamic processes are likely to have at most a limited impact on the measured [234]Th export
448  fluxes.

### 4.1.2. Accounting for non-steady state conditions

450  As the cruise sampling scheme did not allow to collect samples through a time series, it was necessary to assume
451  steady state conditions (i.e., no variation of [234]Th activity with time). However, as documented in previous studies
452  in the west European and Icelandic basins (Buesseler et al., 1992; Martin et al., 2011), this assumption can be
453  questioned as large variations of [234]Th activity were observed at a time scale of one to three weeks along with the
454  onset of the seasonal biological productivity. As a consequence, the SS model was shown to poorly describe the
455  magnitude of the [234]Th export flux, leading to differences with the NSS model up to a factor of 3 (Buesseler et al.,
456  1992; Martin et al., 2011).

457  During the weeks preceding GEOVIDE, large changes in satellite-derived PP were observed (Fig. 4). In order to
458  evaluate the potential error introduced by the SS approach, we attempted to apply a NSS model (see section 2.3;
459  Eq. 4).

460  The west European and Icelandic basins had the highest NSS [234]Th fluxes (3540 dpm m$^{-2}$ d$^{-1}$ at Station 32) while
461  the Irminger basin had the lowest (516 dpm m$^{-2}$ d$^{-1}$ at Station 44; Table 1). The NSS [234]Th fluxes were either larger
462  or similar to those obtained using the SS model. This results from the fact that the NSS approach used here assumes
463  the observed [234]Th activity changes to only reflect a linear decrease from an initial [234]Th activity in secular
464  equilibrium with [238]U, over the time elapsed since the onset of the bloom (Δt, see section 2.3). For stations sampled
465  shortly after the start of the bloom such as in the Irminger, Icelandic and Labrador basins (Δt ranges from 23 to 43
466  days), the fluxes predicted by the NSS model are from 1.4 to 2.1 fold higher than to the SS fluxes. In the west
467  European and Iberian basins, this difference is reduced (NSS fluxes are from 1.1 to 1.3 fold higher) due to a larger
468  Δt, ranging from 48 to 78 days.

469  As a conclusion, the SS export fluxes may have underestimated [234]Th export fluxes at some stations by a maximum
470  factor of 2 such as in the Icelandic basin. Yet, we need to keep in mind that this NSS approach has limitations by
471  assuming the equilibrium between [234]Th and [238]U at the bloom start and by considering only an increasing deficit
472  of [234]Th activity over a given time period (Δt).

### 4.2. Influence of the intensity and stage of the bloom on POC exports

474  The GEOVIDE cruise was carried out in late spring (May-June), a period during which the productivity and the
475  carbon export can be important (Sanders et al., 2014). The [234]Th proxy integrates the activity deficits over a
476  timescale of several weeks preceding the sampling and it appears thus essential to compare the sampling time in
477  light of the bloom development.

478  Apart from Stations 1 and 13, which were sampled after the bloom, the different basins were sampled during the
479  spring bloom, but at different stages. One of the lowest POC export flux was determined at Station 13 in the Iberian
480  basin, where the intensity of the bloom remained rather low along the season (seasonal VGPM-PP=81 mmol m$^{-2}$
481  d$^{-1}$, Fig. 5) due to oligotrophic conditions (depleted nutrients; Fonseca-Batista et al., 2018). In contrast, the highest
482  POC export flux was determined at Station 1, also in the Iberian basin. Station 1 was sampled after the bloom
483  period and satellite-data showed this station was relatively productive in the early spring (185 mmol m$^{-2}$ d$^{-1}$ in
484  March, Fig. 4). This greater POC export observed when the bloom had already declined may be caused by an

ecosystem change, as already described in the Southern Ocean with the emergence of silicified diatoms because of nutrient stress (e.g., Baines et al., 2010; Claquin et al., 2002).

High POC export fluxes were also observed for the west European and Icelandic basins sampled during the bloom. PP appeared maximal just before the sampling in the west European basin (Fig. 4 and 5) and could have promoted these high POC exports. Within the Icelandic basin, both stations were sampled during the productive period, although the peak of the bloom was not yet reached (Fig. 4), suggesting that the export maximum might have occurred later in the season. Both basins have previously been characterized by the presence of fast-sinking particles during the bloom (data from cruises in Spring 2012 and Summer 2009; Villa-Alfageme et al., 2016) promoting the high POC export fluxes.

The Irminger basin was sampled close to the bloom maximum, but unlike the west European and Icelandic basins the POC export flux was low there, probably reflecting accumulation of biomass preceding export. Indeed, this area had the highest *in-situ* PP, a high proportion of particulate $^{234}$Th in surface waters (reaching 94% of the total $^{234}$Th activity at Station 44) and a very low P/J ratio, indicating that $^{234}$Th was retained in the upper waters rather than being exported (Fig. 6; Table 1).

The Labrador Sea basin was sampled just shortly after the peak of PP and was characterized by low *in-situ* PP, low nutrient concentrations, indicating the beginning of the decline of the bloom. The combination of the important PP a few weeks before our sampling (Fig. 4 and 5) and the decline of the bloom likely triggered the high POC export fluxes, as observed elsewhere (Martin et al., 2011; Roca-Marti et al., 2016b; Stange et al., 2016).

Overall, the magnitude of the POC export appears to depend on the degree of progress of the bloom. Indeed, the negative relationship found between the POC export fluxes and the *in-situ* PP relative to the maximal VGPM-PP along the season, representing the bloom stage, highlights that highest export occurs in post bloom periods (Fig. 8), as also evidenced from deep sediment trap studies (Lampitt et al., 2010), and is driven by large and rapidly sinking aggregates (Lampitt et al., 2001; Turner and Millward, 2002).

### 4.3. Influence of the phytoplankton size and community structure on POC exports

In the North Atlantic, the phytoplankton composition varies significantly, depending on the stage of the bloom and on the evolution of environmental parameters such as micro- and macro-nutrient concentrations or stratification depth (Moore et al., 2005). Spatial variations in phytoplankton size structure are known to exert a control on the magnitude of the POC export flux (Boyd and Newton, 1999) and high POC exports are usually related to a greater size of the sinking phytoplankton cells (Alldredge and Silver, 1988; Guidi et al., 2009).

Within the Iberian basin, the highest abundance of pico-phytoplankton was observed at Station 13 (Tonnard et al., in prep.). These conditions are typical of the subtropical and oligotrophic waters (Dortch and Packard, 1989). Villa-Alfageme et al. (2016) highlighted that small cells are usually slow-sinking particles that can be easily remineralised in the upper layers. A small sinking velocity (<100 m d$^{-1}$) allows time for bacteria and zooplankton to degrade such particles, thus reducing the export flux. For the same area, Owens et al. (2014) also report a low flux later in October, confirming a lower carbon export in general in this oligotrophic area. However, Station 1 was characterized by a greater POC export that could be related to the mixed proportion of micro-, nano- and pico-phytoplankton and thus to the greater proportion of larger cells such as diatoms or haptophytes, increasing the particle sinking velocity. The greater POC export there may also be related to the proximity to the margin, where particle dynamics are intense and lithogenic particles are numerous (Gourain et al., 2018).

At higher latitudes, particle sinking velocity has been reported to be high (>100 m d$^{-1}$; Villa-Alfageme et al., 2016), as cells generally are of a larger size. Micro-phytoplankton, with dominance of diatoms, represented an important fraction of the phytoplankton community in the west European, Irminger and Labrador basins and the dense frustules of diatoms have been reported to act as ballast for the sinking organic matter (Klaas and Archer, 2002). Fast-sinking particles could have promoted the relatively high POC export fluxes in those basins. However, in the Icelandic basin, the dominance of nano-phytoplankton coincided with relatively high POC export. Both stations in the Icelandic basin were dominated by haptophytes, including coccolithophorids (Tonnard et al., in prep.). Despite their smaller size, the dense calcium carbonate shells of the latter could promote the export of POC (Francois et al., 2002; Lam et al., 2011).

Our results suggest that high POC export fluxes can be mediated through either micro- or nano-phytopkankton species, suggesting that sinking velocity is influenced by other parameters than the size, likely their composition and density (Fig. 8).

### 4.4. Export and transfer efficiencies of POC

In order to characterize the strength of the biological carbon pump, we used two parameters: the export efficiency (ThE), which is the ratio of the POC export flux at Eq over the PP (Buesseler, 1998) and the transfer efficiency (T100) which is the ratio of the POC export flux at 100 m below Eq over the POC export flux at Eq (Fig. 9). Note that the POC export flux at Eq+100 (Table 3) was calculated by multiplying the $^{234}$Th flux at Eq+100 by the POC to $^{234}$Th ratio of large particles for the same depth. The POC:$^{234}$Th ratio at Eq+100 was deduced from a power law fit (Fig. 3).

Based on *in-situ* PP values (Table 3), ThE ranged from 1 (Station 44) to 38% (Station 69) with a median value of 7% along the transect. The highest export efficiencies were determined at Stations 1 and 69 with values reaching 35 and 38%, respectively. Other stations were characterized by ThE ≤ 14% with highest values (7 – 14%) at Stations 32, 38, 64 and 77. Export efficiencies around 10% are common in the open ocean (Buesseler, 1998). A lower export efficiency can be related to important microbial and zooplankton grazing activities or to biomass accumulation in surface waters (Planchon et al., 2013, 2015). A high ThE can result from many factors such as the presence of large and/or dense and fast sinking particles, low surface remineralisation, active zooplankton migration or nutrient stress (Ceballos-romero et al., 2016; Le Moigne et al., 2016; Planchon et al., 2013). Interestingly, stations with the highest ThE were also characterized by the lowest PP (Stations 1 and 69) while stations with the lowest ThE were characterized by the highest PP (Stations 44 and 51). This inverse relationship between PP and ThE was significant for all stations of the GEOVIDE cruise (regression slope: -0.20; r²=0.58; p<0.01; n=11; Fig. S2) and has been explained in the Southern Ocean by the temporal decoupling between PP and export due to biomass accumulation in surface waters (Henson et al., 2015; Planchon et al., 2013) as well as by other processes such as zooplankton grazing and bacterial activity (Maiti et al., 2013; Le Moigne et al., 2016; Roca-Marti et al., 2016a). Such particle recycling has also been observed in the North Atlantic (Collins et al., 2015; Giering et al., 2014; Marsay et al., 2015) limiting POC export to the deep ocean. A recent study in the Icelandic and Irminger basins highlights the impact of the bloom dynamics on the particle export efficiency resulting in strong seasonal variability of the ThE (Ceballos-Romero et al., 2016). Our estimates are generally in the lower range of export efficiencies reported by others for the North Atlantic with values ranging from 1 to 42% in the western European basin (Buesseler et al., 1992; Lampitt et al., 2008; Thomalla et al., 2008), from 5 to 8%

in the Icelandic basin (Ceballos-romero et al., 2016), from 4 to 16% in the Irminger basin (Ceballos-romero et al., 2016) and from 4 to > 100% in the Labrador basin (Moran et al., 2003). This wide range confirms that export efficiencies are highly variable in the North Atlantic in late spring. The overall low export efficiency of the North Atlantic is characteristic of highly productive areas of the world ocean.

However, it should be kept in mind that the ThE calculation is based on two parameters that are integrating processes over different time scales: 24 h for *in-situ* PP and several weeks for export. Strong variability of PP during this longer period would highly impact the ThE ratio. Therefore, ThE ratios were also estimated using the VGPM-derived 8-day, 32-day and seasonal PP (Table 3). As seen in Section 2.7, there are no significant differences between the VGPM-PP estimates regardless of the integrations times, and thus no significant differences between the corresponding ThE values. Stations 1 and 69 are exceptions with ThE values decreasing from 35 to 12% and from 38 to 8%, respectively, due to unusually low *in-situ* PP during our study which led to over-estimated ThE.

Carbon transfer efficiencies (T100) ranged from 30 (Station 69) to 78% (Station 32). Generally, the fluxes at these greater depths were characterized by greater error bars (see Fig. 9) due to the increasing uncertainty of the $^{234}$Th fluxes with increasing depth. The highest T100 were observed within the Icelandic basin with values reaching 78 and 74% at Stations 32 and 38 respectively. On the contrary, the lowest T100 values were observed at Stations 1, 13, 21 and 69 (between 30 and 49%) highlighting greater carbon remineralisation between Eq and Eq+100 m at these latter stations, as well as confirming important regional variability of the transfer efficiency as reported also by others (Lam et al., 2011; Lutz et al., 2002). The low T100 (and high R100) values observed in the eastern part of the transect (Stations 1, 13 and, to a lesser extent Station 21) likely reflect an important bacterial activity in these warmer waters (>13°C in the upper 100 m; Iversen and Ploug, 2013; Marsay et al., 2015; Rivkin and Legendre, 2001), efficiently degrading the probably slow-sinking particles. Such recycling is characteristic for regeneration-based microbial food webs in oligotrophic regimes (Karl, 1999; Thomalla et al., 2006). In the Icelandic basin, the high T100 may be related to the large abundance of coccolithophorids (Tonnard et al., in prep.) known to enhance the POC transfer due to their ballasting effect (Francois et al., 2002; Lam et al., 2011). Indeed, Bach et al. (2016) found that a bloom of coccolithophorids can increase the transfer efficiency through the mesopelagic layer by 14-24%. Finally, the Labrador and Irminger basins exhibit relatively similar T100 (between 50 and 69%), except at Station 69 where the lowest T100 was observed. This is also in agreement with the highest R100 and carbon remineralisation flux determined with the Ba$_{xs}$ proxy (Lemaitre et al., 2018). The central Labrador basin, in proximity of Station 69, was characterized by strong subduction of the LSW during the winter preceding the GEOVIDE cruise. This downwelling could have promoted an important organic matter export leading to important prokaryotic heterotrophic activity in mesopelagic waters. This enhanced remineralisation was still observed during GEOVIDE as traced by a large mesopelagic Ba$_{xs}$ content (Lemaitre et al., 2018).

## 5. Conclusion

Overall, POC export varied by a factor of ~ 9 along the transect highlighting an important spatial variation. POC flux results obtained from other studies in the North Atlantic range from similar to up to 27 times larger values, with rapid changes over a month duration, confirming the large temporal variability of the POC export fluxes.

600  The magnitude of the POC export seems to be associated with the state of the bloom. Accumulation of biomass in
601  surface waters during the bloom may induce a limitation of the POC export flux while during the post bloom
602  period increasing numbers of rapidly sinking particles increases POC export.

603  The magnitude of the fluxes seems also related to the phytoplankton size and community structure. One of the
604  lowest POC export fluxes was found at the stations where pico-phytoplankton dominated the community. In
605  contrast, the areas composed by micro- and nano-phytoplankton were characterized by high POC export fluxes.
606  These areas were dominated by diatoms or coccolithophorids, known to strongly ballast the POC export fluxes.
607  This suggests that the size as well as the composition and density of the particles likely play an important role on
608  the particulate sinking velocities and thus on the magnitude of the POC export fluxes.

609  For most stations, the fraction of primary production that is exported from the surface zone (export efficiency) was
610  $\leq 14\%$, which is in agreement with the global ocean export efficiency (~10%; Buesseler, 1998). Export efficiency
611  was also inversely related to primary production, indicating that the North Atlantic during our study behaved like
612  most of the highly productive areas of the world's ocean, with a low export efficiency. Finally, the fraction of POC
613  that is not remineralised in the mesopelagic zone (transfer efficiency) fits within the range of measured transfer
614  efficiencies reported elsewhere (e.g., Black et al., 2017; Buesseler and Boyd, 2009). The highest transfer
615  efficiencies were determined at the stations where coccolithophorids dominated.

616  **Acknowledgements**

617  We would like to thank the captain and the crew of the R/V Pourquoi Pas?, the chief scientists Pascale Lherminier
618  and Géraldine Sarthou, as well as Fabien Perault and Emmanuel De Saint Léger (CNRS DT-INSU), Pierre
619  Branellec, Michel Hamon, Catherine Kermabon, Philippe Le Bot, Stéphane Leizour and Olivier Ménage
620  (Laboratoire d'Océanographie Physique et Spatiale) for their technical expertise during ISP and CTD deployments
621  and Catherine Schmechtig for the GEOVIDE database management. We also acknowledge Emilie Grossteffan,
622  Manon Le Goff, Morgane Galinari and Paul Tréguer for the analysis of nutrients. Special thanks to Maxi Castrillejo
623  (UAB, Spain), Catherine Jeandel (LEGOS, France), Virginie Sanial (WHOI, USA), Raphaëlle Sauzède (LOV,
624  France) and Lorna Foliot (LSCE, France) for their help at sea and for the ISP coordination. We would also like to
625  thank Phoebe Lam for providing two modified McLane ISP. Laurence Monin (MRAC, Belgium), David
626  Verstraeten, Claire Mourgues and Martine Leermarkers (VUB, Belgium) greatly helped during sample processing
627  and element analysis by ICP-MS and EA-IRMS. Audrey Plante (ULB, Belgium) and Emilie Le Roy (LEGOS,
628  France) assisted with the counting of the residual Thorium-234 activities. Satellite primary production data and
629  visualizations used in this study were produced with the Ocean Productivity website at Oregon State University.
630  This work was funded by the Flanders Research Foundation (project G071512N), the Vrije Universiteit Brussel
631  (Strategic Research Program, project SRP-2), the French ANR Blanc GEOVIDE (ANR-13-BS06-0014), ANR
632  RPDOC BITMAP (ANR-12-PDOC-0025-01), IFREMER, CNRS-INSU (programme LEFE), INSU OPTIMISP
633  and Labex-Mer (ANR-10-LABX-19).

634  **References**

635  Alldredge, A. L. and Silver, M. W.: Characteristics, dynamics and significance of marine snow, Prog. Oceanogr.,
636  20, 41–82, 1988.

637    Aminot, A. and Kérouel, R.: Dosage automatique des nutriments dans les eaux marines: méthodes en flux continu,
638    Ifremer-Qu., 2007.

639    Bach, L. T., Boxhammer, T., Larsen, A., Hildebrandt, N., Schulz, K. G. and Riebesell, U.: Influence of plankton
640    community structure on the sinking velocity of marine aggregates, Global Biogeochem. Cycles, 30, 1145–1165,
641    doi:10.1002/2016GB005372, 2016.

642    Baines, S. B., Twining, B. S., Brzezinski, M. A., Nelson, D. M. and Fisher, N. S.: Causes and biogeochemical
643    implications of regional differences in silification of marine diatoms, Global Biogeochem. Cycles, 24(4), 1–15,
644    doi:10.1029/2010GB003856, 2010.

645    Behrenfeld, M. and Falkowski, P. G.: A consumer's guide to phytoplankton primary productivity models, Limnol.
646    Oceanogr., 42(7), 1479–1491, doi:10.4319/lo.1997.42.7.1479, 1997.

647    Behrenfeld, M. J., Boss, E., Siegel, D. A. and Shea, D. M.: Carbon-based ocean productivity and phytoplankton
648    physiology from space, Global Biogeochem. Cycles, 19(1), 1–14, doi:10.1029/2004GB002299, 2005.

649    Benitez-Nelson, C. R., Buesseler, K. O. and Crossin, G.: Upper ocean carbon export, horizontal transport, and
650    vertical eddy diffusivity in the southwestern Gulf of Maine, Cont. Shelf Res., 20(6), 707–736, doi:10.1016/S0278-
651    4343(99)00093-X, 2000.

652    Bhat, S. G., Krishnaswanmy, S., Lal, D. and Moore, W. S.: 234Th/238U Ratios in the Ocean, Earth Planet. Sci.
653    Lett., 5, 433–491, 1969.

654    Black, E. E., Buesseler, K. O., Pike, S. M. and Lam, P. J.: 234Th as a tracer of particulate export and
655    remineralization    in    the    southeastern    tropical    Pacific,    Mar.    Chem.,    (June),    1–16,
656    doi:10.1016/j.marchem.2017.06.009, 2017.

657    Boyd, P. W. and Newton, P. P.: Does planktonic community structure determine downward particulate organic
658    carbon flux in different oceanic provinces ?, Deep Sea Res. Part I Oceanogr. Res. Pap., 46, 63–91, 1999.

659    Buesseler, K. O.: The decoupling of production and particulate export in the surface ocean, Global Biogeochem.
660    Cycles, 12(2), 297, doi:10.1029/97GB03366, 1998.

661    Buesseler, K. O. and Boyd, P. W.: Shedding light on processes that control particle export and flux attenuation in
662    the twilight zone of the open ocean, Limnol. Oceanogr., 54(4), 1210–1232, doi:10.4319/lo.2009.54.4.1210, 2009.

663    Buesseler, K. O., Bacon, M. P., Kirk Cochran, J. and Livingston, H. D.: Carbon and nitrogen export during the
664    JGOFS North Atlantic Bloom experiment estimated from 234Th: 238U disequilibria, Deep Sea Res. Part A.
665    Oceanogr. Res. Pap., 39(7–8), 1115–1137, doi:10.1016/0198-0149(92)90060-7, 1992.

666    Buesseler, K. O., Andrews, J. A., Hartman, M. C., Belastock, R. and Chai, F.: Regional estimates of the export
667    flux of particulate organic carbon derived from thorium-234 during the JGOFS EqPac program, Deep Sea Res.
668    Part II Top. Stud. Oceanogr., 42(2–3), 777–804, doi:10.1016/0967-0645(95)00043-P, 1995.

669    Buesseler, K. O., Benitez-Nelson, C. R., Moran, S. B., Burd,  a., Charette, M., Cochran, J. K., Coppola, L., Fisher,
670    N. S., Fowler, S. W., Gardner, W. D., Guo, L. D., Gustafsson, Ö., Lamborg, C., Masque, P., Miquel, J. C., Passow,
671    U., Santschi, P. H., Savoye, N., Stewart, G. and Trull, T.: An assessment of particulate organic carbon to thorium-
672    234 ratios in the ocean and their impact on the application of 234Th as a POC flux proxy, Mar. Chem., 100(3–4
673    SPEC. ISS.), 213–233, doi:10.1016/j.marchem.2005.10.013, 2006.

674    Buesseler, K. O., Trull, T. W., Steinberg, D. K., Silver, M. W., Siegel, D. a., Saitoh, S. I., Lamborg, C. H., Lam,
675    P. J., Karl, D. M., Jiao, N. Z., Honda, M. C., Elskens, M., Dehairs, F., Brown, S. L., Boyd, P. W., Bishop, J. K. B.
676    and Bidigare, R. R.: VERTIGO (VERtical Transport In the Global Ocean): A study of particle sources and flux
677    attenuation    in    the    North    Pacific,    Deep    Sea    Res.    Part    II    Top.    Stud.    Oceanogr.,    55(14–15),    1522–1539,
678    doi:10.1016/j.dsr2.2008.04.024, 2008.

679    Cai, P., Rutgers Van Der Loeff, M., Stimac, I., Nthig, E. M., Lepore, K. and Moran, S. B.: Low export flux of
680    particulate organic carbon in the central Arctic Ocean as revealed by 234Th:238U disequilibrium, J. Geophys.
681    Res. Ocean., 115(10), 1–21, doi:10.1029/2009JC005595, 2010.

682    Ceballos-romero, E., Le Moigne, F. A. C., Henson, S., Marsay, C. M., Sanders, R. J., García-Tenorio, R. and Villa-

Alfageme, M.: Influence of bloom dynamics on particle export efficiency in the North Atlantic: a comparative study of radioanalytical techniques and sediment traps, Mar. Chem., 186, 198–210, doi:10.1016/j.marchem.2016.10.001, 2016.

Claquin, P., Martin-Jézéquel, V., Kromkamp, J. C., Veldhuis, M. J. W. and Kraay, G. W.: Uncoupling of silicon compared with carbon and nitrogen metabolisms and the role of the cell cycle in continuous cultures of Thalassiosira pseudonana (Bacillariophyceae) under light, nitrogen, and phosphorus control, J. Phycol., 38(5), 922–930, doi:10.1046/j.1529-8817.2002.t01-1-01220.x, 2002.

Coale, K. H. and Bruland, K. W.: Thorium-234:uranium-238 disequilibria within the California Current, Limnol. Oceanogr., 30(l), 22–33, doi:10.4319/lo.1985.30.1.0022, 1985.

Cochran, J. K. and Masqué, P.: Short-lived U/Th series radionuclides in the ocean: Tracers for scavenging rates, export fluxes and particle dynamics, Rev. Mineral. Geochemistry, 52, 461–492, doi:10.2113/0520461, 2003.

Collins, J. R., Edwards, B. R., Thamatrakoln, K., Ossolinski, J. E., Ditullio, G. R., Bidle, K. D., Doney, S. C. and Mooy, B. A. S. Van: The multiple fates of sinking particles in the North Atlantic Ocean, Global Biogeochem. Cycles, 29, 1471–1494, doi:10.1002/2014GB005037, 2015.

Costa Goela, P., Cordeiro, C., Danchenko, S., Icely, J., Cristina, S. and Newton, A.: Time series analysis of data for sea surface temperature and upwelling components from the southwest coast of Portugal, J. Mar. Syst., 163, 12–22, doi:10.1016/j.jmarsys.2016.06.002, 2016.

Dortch, Q. and Packard, T. T.: Differences in biomass structure between oligotrophic and eutrophic marine ecosystems, Deep Sea Res. Part A. Oceanogr. Res. Pap., 36(2), 223–240, 1989.

Eppley, R. W.: Temperature and phytoplankton growth in the sea, Fish. Bull., 70(4), 1063–1085, 1972.

Esaias, W. E., Feldman, G. C., MnClain, C. R. and Elrod, J. A.: Monthly satellite-derived phytoplankton pigment distribution for the North Atlantic basin, Ocenaography Rep., 67(44), 835–837, 1986.

Ferron, B., Kokoszka, F., Mercier, H. and Lherminier, P.: Dissipation rate estimates from microstructure and finescale internal wave observations along the A25 Greenland-Portugal OVIDE line, J. Atmos. Ocean. Technol., 31(11), 2530–2543, doi:10.1175/JTECH-D-14-00036.1, 2014.

Fonseca-Batista, D., Li, X., Riou, V., Michotey, V., Fripiat, F., Deman, F., Guasco, S., Brion, N., Lemaitre, N., Planchon, F., Tonnard, M., Planquette, H., Gallinari, M., Sarthou, G., Elskens, M., Chou, L. and Dehairs, F.: Evidence of high N2 fixation rates in productive waters of the temperate Northeast Atlantic, Biogeosciences, 2018.

Francois, R., Honjo, S., Krishfield, R. and Manganini, S.: Factors controlling the flux of organic carbon to the bathypelagic zone of the ocean, Global Biogeochem. Cycles, 16(4), 1–20, doi:10.1029/2001GB001722, 2002.

GEOTRACES: GEOTRACES (an international study of the marine biogeochemical cycle of trace elements and isotopes): Science Plan., 2006.

Giering, S. L. C., Sanders, R., Lampitt, R. S., Anderson, T. R., Tamburini, C., Boutrif, M., Zubkov, M. V, Marsay, C. M., Henson, S. A., Saw, K., Cook, K. and Mayor, D. J.: Reconciliation of the carbon budget in the ocean's twilight zone, Nature, 507(7493), 480–483, doi:10.1038/nature13123, 2014.

Giering, S. L. C., Sanders, R., Martin, A. P., Lindemann, C., Möller, K. O., Daniels, C. J., Mayor, D. J. and St. John, M. A.: High export via small particles before the onset of the Nort Atlantic spring bloom, J. Geophys. Res., 121, 1–17, doi:10.1002/2016JC012048.Received, 2016.

Gourain, A., Planquette, H., Cheize, M., Menzel, J.-L., Boutorh, J., Shelley, R., Pereira Contraira, L., Lemaitre, N., Lacan, F., Lherminier, P. and Sarthou, G.: Particulate trace metals along the GEOVIDE section, Biogeosciences, 2018.

Guidi, L., Stemmann, L., Jackson, G. A., Ibanez, F., Claustre, H., Legendre, L., Picheral, M. and Gorsky, G.: Effects of phytoplankton community on production , size and export of large aggregates : A world-ocean analysis, Limnol. Oceanogr., 54(6), 1951–1963, 2009.

Guidi, L., Legendre, L., Reygondeau, G., Uitz, J., Stemmann, L. and Henson, S. A.: A new look at ocean carbon remineralization for estimating deepwater sequestration, Glob. Planet. Change, 29, 1044–1059,

729     doi:10.1002/2014GB005063.Received, 2015.

730     Hall, I. R., Schmidt, S., McCave, I. N. and Reyss, J. L.: Particulate matter distribution and 234Th/238U
731     disequilibrium along the Northern Iberian Margin : implications for particulate organic carbon export, Deep. Res.
732     Part I, 47, 557–582, 2000.

733     Hama, T., Miyazaki, T., Ogawa, Y., Iwakuma, T., Takahashi, M., Otsuki, A. and Ichimura, S.: Mesurement of
734     photosynthtic production of a marine phytoplankton population using a stable 13C isotope, Mar. Biol., 73, 31–36,
735     1983.

736     Henson, S. A., Dunne, J. P. and Sarmiento, J. L.: Decadal variability in North Atlantic phytoplankton blooms, J.
737     Geophys. Res., 114(C4), C04013–C04013, doi:10.1029/2008JC005139, 2009.

738     Henson, S. A., Sanders, R. and Madsen, E.: Global patterns in efficiency of particulate organic carbon export and
739     transfer to the deep ocean, Global Biogeochem. Cycles, 26(1), 1–14, doi:10.1029/2011GB004099, 2012.

740     Henson, S. A., Yool, A. and Sanders, R.: Variability in efficiency of particulate organic carbon export: a model
741     study, Global Biogeochem. Cycles, 29, 33–45, doi:10.1002/2014GB004965.Received, 2015.

742     Herndl, G. J. and Reinthaler, T.: Microbial control of the dark end of the biological pump, Nat. Geosci., 6(9), 718–
743     724, doi:10.1038/ngeo1921, 2013.

744     Honjo, S. and Manganini, S. J.: Annual biogenic particle fluxes to the interior of the North Atlantic Ocean; studied
745     at 34°N 21°W and 48°N 21°W, Deep Sea Res. Part I Oceanogr. Res. Pap., 40(1), 587–607, 1993.

746     Iversen, M. H. and Ploug, H.: Temperature effects on carbon-specific respiration rate and sinking velocity of
747     diatom aggregates – potential implications for deep ocean export processes, Biogeosciences, 10, 4073–4085,
748     doi:10.5194/bg-10-4073-2013, 2013.

749     Karl, D. M.: A Sea of change: Biogeochemical variability in the North Pacific Subtropical Gyre, Ecosystems, 2,
750     181–214, 1999.

751     Kieke, D. and Yashayaev, I.: Studies of Labrador Sea Water formation and variability in the subpolar North
752     Atlantic in the light of international partnership and collaboration, Prog. Oceanogr., 132, 220–232,
753     doi:10.1016/j.pocean.2014.12.010, 2015.

754     Klaas, C. and Archer, D. E.: Association of sinking organic matter with various types of mineral ballast in the deep
755     sea: Implications for the rain ratio, Global Biogeochem. Cycles, 16(4), 1–14, doi:10.1029/2001GB001765, 2002.

756     Lam, P. J., Doney, S. C. and Bishop, J. K. B.: The dynamic ocean biological pump: Insights from a global
757     compilation of particulate organic carbon, CaCO3, and opal concentration profiles from the mesopelagic, Global
758     Biogeochem. Cycles, 25(3), 1–14, doi:10.1029/2010GB003868, 2011.

759     Lampitt, R. S., Bett, B. J., Kiriakoulakis, K., Popova, E. E., Ragueneau, O., Vangriesheim, A. and Wolff, G. A.:
760     Material supply to the abyssal seafloor in the Northeast Atlantic, Prog. Oceanogr., 50, 27–63, 2001.

761     Lampitt, R. S., Boorman, B., Brown, L., Lucas, M., Salter, I., Sanders, R., Saw, K., Seeyave, S., Thomalla, S. J.
762     and Turnewitsch, R.: Particle export from the euphotic zone: Estimates using a novel drifting sediment trap, 234Th
763     and new production, Deep Sea Res. Part I Oceanogr. Res. Pap., 55(11), 1484–1502, doi:10.1016/j.dsr.2008.07.002,
764     2008.

765     Lampitt, R. S., Salter, I., de Cuevas, B. A., Hartman, S., Larkin, K. E. and Pebody, C. A.: Long-term variability of
766     downward particle flux in the deep northeast Atlantic: Causes and trends, Deep Sea Res. Part II Top. Stud.
767     Oceanogr., 57(15), 1346–1361, doi:10.1016/j.dsr2.2010.01.011, 2010.

768     Lemaitre, N., Planquette, H., Planchon, F., Sarthou, G., Jacquet, S., García-Ibáñez, M. I., Gourain, A., Cheize, M.,
769     Monin, L., André, L., Laha, P., Terryn, H. and Dehairs, F.: Particulate barium tracing significant mesopelagic
770     carbon remineralisation in the North Atlantic, Biogeosciences, 2018.

771     Lemaitre, N., Planquette, H., Planchon, F., Dehairs, F., Roig, S. and Sarthou, G.: High variability of export fluxes
772     along the North Atlantic GEOTRACES section GA01: Importance of minerals as ballast of particulate organic
773     carbon export., in prep., n.d.

Lima, I. D., Lam, P. J. and Doney, S. C.: Dynamics of particulate organic carbon flux in a global ocean model, Biogeosciences, 11(4), 1177–1198, doi:10.5194/bg-11-1177-2014, 2014.

Longhurst, A. R.: Ecological geography of the sea, Academic P., San Diego., 2010.

Lutz, M., Dunbar, R. and Caldeira, K.: Regional variability in the vertical flux of particulate organic carbon in the ocean interior, Global Biogeochem. Cycles, 16(3), 1–15, doi:10.1029/2000GB001383, 2002.

Maiti, K., Benitez-Nelson, C. R. and Buesseler, K. O.: Insights into particle formation and remineralization using the short-lived radionuclide, Thoruim-234, Geophys. Res. Lett., 37(May), 2–7, doi:10.1029/2010GL044063, 2010.

Maiti, K., Charette, M. A., Buesseler, K. O. and Kahru, M.: An inverse relationship between production and export efficiency in the Southern Ocean, Geophys. Res. Lett., 40(8), 1557–1561, doi:10.1002/grl.50219, 2013.

Marsay, C. M., Sanders, R. J., Henson, S. A., Pabortsava, K., Achterberg, E. P. and Lampitt, R. S.: Attenuation of sinking particulate organic carbon flux through the mesopelagic ocean., Proc. Natl. Acad. Sci. U. S. A., 112(4), 1089–1094, doi:10.1073/pnas.1415311112, 2015.

Martin, P., Lampitt, R. S., Jane Perry, M., Sanders, R., Lee, C. and D'Asaro, E.: Export and mesopelagic particle flux during a North Atlantic spring diatom bloom, Deep Sea Res. Part I Oceanogr. Res. Pap., 58(4), 338–349, doi:10.1016/j.dsr.2011.01.006, 2011.

Mercier, H., Lherminier, P., Sarafanov, A., Gaillard, F., Daniault, N., Desbruyères, D., Falina, A., Ferron, B., Gourcuff, C., Huck, T. and Thierry, V.: Variability of the meridional overturning circulation at the Greenland-Portugal OVIDE section from 1993 to 2010, Prog. Oceanogr., 132, 250–261, doi:10.1016/j.pocean.2013.11.001, 2015.

Le Moigne, F. A. C., Sanders, R. J., Villa-Alfageme, M., Martin, A. P., Pabortsava, K., Planquette, H., Morris, P. J. and Thomalla, S. J.: On the proportion of ballast versus non-ballast associated carbon export in the surface ocean, Geophys. Res. Lett., 39(15–16), L15610–L15610, doi:10.1029/2012GL052980, 2012.

Le Moigne, F. A. C., Villa-Alfageme, M., Sanders, R. J., Marsay, C., Henson, S. and García-Tenorio, R.: Export of organic carbon and biominerals derived from 234Th and 210Po at the Porcupine Abyssal Plain, Deep Sea Res. Part I Oceanogr. Res. Pap., 72(August), 88–101, doi:10.1016/j.dsr.2012.10.010, 2013a.

Le Moigne, F. A. C., Henson, S. A., Sanders, R. J. and Madsen, E.: Global database of surface ocean particulate organic carbon export fluxes diagnosed from the 234-Th technique, Earth Syst. Sci. Data, 5(2), 295–304, doi:10.5194/essd-5-295-2013, 2013b.

Le Moigne, F. A. C., Henson, S. A., Cavan, E. L., Georges, C., Pabortsava, K., Achterberg, E. P., Ceballos-romero, E. and Zubkov, M.: What causes the inverse relationship between primary production and export efficiency in the Southern Ocean?, Geophys. Res. Lett., 43, 1–10, doi:10.1002/2016GL068480.Received, 2016.

Moore, C. M., Lucas, M. I., Sanders, R. and Davidson, R.: Basin-scale variability of phytoplankton bio-optical characteristics in relation to bloom state and community structure in the Northeast Atlantic, Deep Sea Res. Part I Oceanogr. Res. Pap., 52, 401–419, doi:10.1016/j.dsr.2004.09.003, 2005.

Moore, C. M., Mills, M. M., Langlois, R., Milne, A., Achterberg, E. P., Roche, J. La and Geider, R. J.: Relative influence of nitrogen and phosphorus availability on phytoplankton physiology and productivity in the oligotrophic sub-tropical North Atlantic Ocean, Limnol. Oceanogr., 53(1), 291–305, 2008.

Moran, S. B., Weinstein, S. E., Edmonds, H. N., Smith, J. N., Kelly, R. P., Pilson, M. E. Q. and Harrison, W. G.: Does 234Th/238U disequilibrium provide an accurate record of the export flux of particulate organic carbon from the upper ocean?, Limnol. Oceanogr., 48(3), 1018–1029, doi:10.4319/lo.2003.48.3.1018, 2003.

Mouw, C. B., Barnett, A., Mckinley, G. A., Gloege, L. and Pilcher, D.: Phytoplankton size impact on export flux in the global Ocean, Global Biogeochem. Cycles, 30, 1542–1562, doi:10.1002/2015GB005355, 2016.

Owens, S. A., Buesseler, K. O. and Sims, K. W. W.: Re-evaluating the 238U-salinity relationship in seawater: Implications for the 238U-234Th disequilibrium method, Mar. Chem., 127(1–4), 31–39, doi:10.1016/j.marchem.2011.07.005, 2011.

Owens, S. A., Pike, S. and Buesseler, K. O.: Thorium-234 as a tracer of particle dynamics and upper ocean export

820  in the Atlantic Ocean, Deep Sea Res. Part II Top. Stud. Oceanogr., 116, 42–59, doi:10.1016/j.dsr2.2014.11.010,
821  2014.

822  Pike, S., Buesseler, K. O., Andrews, J. and Savoye, N.: Quantification of 234Th recovery in small volume seawater
823  samples by Inductively Coupled Plasma Mass Spectrometry, J. Radioanal. Nucl. Chem., 263, 355–360, 2005.

824  Planchon, F., Cavagna, A.-J., Cardinal, D., André, L. and Dehairs, F.: Late summer particulate organic carbon
825  export and twilight zone remineralisation in the Atlantic sector of the Southern Ocean, Biogeosciences, 10(2),
826  803–820, doi:10.5194/bg-10-803-2013, 2013.

827  Planchon, F., Ballas, D., Cavagna, A.-J., Bowie, A. R., Davies, D. M., Trull, T., Laurenceau, E. C., van der Merwe,
828  P. and Dehairs, F.: Carbon export in the naturally iron-fertilized Kerguelen area of the Southern Ocean based on
829  the 234 Th approach, Biogeosciences, 12, 3831–3848, doi:10.5194/bgd-12-3831-2015, 2015.

830  Puigcorbé, V., Roca-Martí, M., Masqué, P., Benitez-Nelson, C., Rutgers van der Loeff, M., Bracher, A. and
831  Moreau, S.: Latitudinal distributions of particulate carbon export across the North Western Atlantic Ocean, Deep
832  Sea Res. Part I Oceanogr. Res. Pap., doi:10.1016/j.dsr.2017.08.016, 2017.

833  Ras, J., Claustre, H. and Uitz, J.: Spatial variability of phytoplankton pigment distributions in the Subtropical South
834  Pacific Ocean: comparison between in situ and predicted data, Biogeosciences, 5, 353–369, 2008.

835  Resplandy, L., Martin, A. P., Le Moigne, F., Martin, P., Aquilina, A., M??mery, L., L??vy, M. and Sanders, R.:
836  How does dynamical spatial variability impact 234Th-derived estimates of organic export?, Deep Sea Res. Part I
837  Oceanogr. Res. Pap., 68, 24–45, doi:10.1016/j.dsr.2012.05.015, 2012.

838  Reverdin, G., Niiler, P. P. and Valdimarsson, H.: North Atlantic Ocean surface currents, J. Geophys. Res., 108, 1–
839  21, doi:10.1029/2001JC001020, 2003.

840  Riley, G.: Phytoplankton of the North Central Sargasso Sea, 1950-52, Limnol. Oceanogr., 2, 252–270,
841  doi:10.1002/lno.1957.2.3.0252, 1957.

842  Rivkin, R. B. and Legendre, L.: Biogenic carbon cycling in the upper ocean: Effects of microbial respiration,
843  Science (80-. )., 291, 2398–2400, 2001.

844  Roca-Marti, M., Puigcorbé, V., van der Loeff, M. R., Katlein, C., Fernandez-Mendez, M., Peeken, I. and Masqué,
845  P.: Carbon export fluxes and export efficiency in the central Arctic during the record sea-ice minimum in 2012: a
846  joint 234Th/238U and 210Po/210Pb study, J. Geophys. Res., 121, 1–20, doi:10.1002/2016JC011816.Received,
847  2016a.

848  Roca-Marti, M., Puigcorbé, V., Iversen, M. H., van der Loeff, M. R., Klaas, C., Cheah, W., Bracher, A. and
849  Masqué, P.: High particulate organic carbon export during the decline of a vast diatom bloom in the Atlantic sector
850  of the Southern Ocean, Deep Sea Res. Part II Top. Stud. Oceanogr., doi:10.1016/j.dsr2.2015.12.007, 2016b.

851  Rutgers van der Loeff, M., Cai, P. H., Stimac, I., Bracher, A., Middag, R., Klunder, M. B. and van Heuven, S. M.
852  A. C.: 234Th in surface waters: Distribution of particle export flux across the Antarctic Circumpolar Current and
853  in the Weddell Sea during the GEOTRACES expedition ZERO and DRAKE, Deep. Res. Part II Top. Stud.
854  Oceanogr., 58(25–26), 2749–2766, doi:10.1016/j.dsr2.2011.02.004, 2011.

855  Rutgers van der Loeff, M. M., Sarin, M. M., Baskaran, M., Benitez-Nelson, C., Buesseler, K. O., Charette, M.,
856  Dai, M., Gustafsson, Ö., Masque, P., Morris, P. J., Orlandini, K., Rodriguez y Baena, A., Savoye, N., Schmidt, S.,
857  Turnewitsch, R., Vöge, I. and Waples, J. T.: A review of present techniques and methodological advances in
858  analyzing  234Th  in  aquatic  systems,  Mar.  Chem.,  100(3–4  SPEC.  ISS.),  190–212,
859  doi:10.1016/j.marchem.2005.10.012, 2006.

860  Sanders, R., Morris, P. J., Poulton, A. J., Stinchcombe, M. C., Charalampopoulou, A., Lucas, M. I. and Thomalla,
861  S. J.: Does a ballast effect occur in the surface ocean ?, Geophys. Res. Lett., 37, 1–5, doi:10.1029/2010GL042574,
862  2010.

863  Sanders, R., Henson, S. A., Koski, M., La, C. L. De, Painter, S. C., Poulton, A. J., Riley, J., Salihoglu, B., Visser,
864  A., Yool, A., Bellerby, R. and Martin, A. P.: The Biological Carbon Pump in the North Atlantic, Prog. Oceanogr.,
865  129, 200–218, doi:10.1016/j.pocean.2014.05.005, 2014.

866  Savoye, N., Buesseler, K. O., Cardinal, D. and Dehairs, F.: 234 Th deficit and excess in the Southern Ocean during
867  spring 2001: Particle export and remineralization, Geophys. Res. Lett., 31(12), L12301–L12301,
868  doi:10.1029/2004GL019744, 2004.

869  Savoye, N., Benitez-Nelson, C., Burd, A. B., Cochran, J. K., Charette, M., Buesseler, K. O., Jackson, G. A., Roy-
870  Barman, M., Schmidt, S. and Elskens, M.: 234Th sorption and export models in the water column: A review, Mar.
871  Chem., 100, 234–249, doi:10.1016/j.marchem.2005.10.014, 2006.

872  Shelley, R. U., Roca-Martí, M., Castrillejo, M., Masqué, P., Landing, W. M., Planquette, H. and Sarthou, G.:
873  Quantification of trace element atmospheric deposition fluxes to the Atlantic Ocean (>40°N; GEOVIDE,
874  GEOTRACES GA01) during spring 2014, Deep Sea Res. Part I Oceanogr. Res. Pap., (June),
875  doi:10.1016/j.dsr.2016.11.010, 2016.

876  Stange, P., Bach, L. T., Le Moigne, F. A. C., Taucher, J., Boxhammer, T. and Riebesell, U.: Quantifying the time
877  lag between organic matter production and export in the surface ocean: Implications for estimates of export
878  efficiency, Geophys. Res. Lett., 43, 1–9, doi:10.1002/2016GL070875, 2016.

879  Thomalla, S., Turnewitsch, R., Lucas, M. and Poulton, A.: Particulate organic carbon export from the North and
880  South Atlantic gyres: The 234Th/238U disequilibrium approach, Deep Sea Res. Part II Top. Stud. Oceanogr., 53,
881  1629–1648, doi:10.1016/j.dsr2.2006.05.018, 2006.

882  Thomalla, S. J., Poulton, A. J., Sanders, R., Turnewitsch, R., Holligan, P. M. and Lucas, M. I.: Variable export
883  fluxes and efficiencies for calcite, opal, and organic carbon in the Atlantic Ocean: A ballast effect in action ?,
884  Global Biogeochem. Cycles, 22, 1–10, doi:10.1029/2007GB002982, 2008.

885  Tonnard, M., Donval, A., Lampert, L., Claustre, H., Ras, J., Dimier, C., Sarthou, G., Planquette, H., van der Merwe,
886  P., Boutorh, J., Cheize, M., Menzel, J.-L., Pereira Contraira, L., Shelley, R., Bowie, A. R., Tréguer, P., Gallinari,
887  M., Duprez de Gesincourt, F., Germain, Y. and Lherminier, P.: Phytoplankton assemblages along the GEOVIDE
888  section (GEOTRACES section GA01) using CHEMTAX, n.d.

889  Turner, A. and Millward, G. E.: Suspended Particles: Their Role in Estuarine Biogeochemical Cycles, Estuar.
890  Coast. Shelf Sci., 55(6), 857–883, doi:10.1006/ecss.2002.1033, 2002.

891  Villa-Alfageme, M., Soto, F. C., Ceballos, E., Giering, S. L. C., Le Moigne, F. A. C., Henson, S., Mas, J. L. and
892  Sanders, R. J.: Geographical, seasonal and depth variation in sinking particle speeds in the North Atlantic,
893  Geophys. Res. Lett., 43, 8609–8616, doi:10.1002/2016GL069233.Received, 2016.

894  Westberry, T., Behrenfeld, M. J., Siegel, D. A. and Boss, E.: Carbon-based primary productivity modeling with
895  vertically resolved photoacclimation, Global Biogeochem. Cycles, 22(2), 1–18, doi:10.1029/2007GB003078,
896  2008.

897  Zehr, J. P. and Ward, B. B.: Nitrogen Cycling in the Ocean : New Perspectives on Processes and Paradigms
898  MINIREVIEW Nitrogen Cycling in the Ocean : New Perspectives on Processes and Paradigms, Appl. Environ.
899  Microbiol., 68(3), 1015–1024, doi:10.1128/AEM.68.3.1015, 2002.

900  Zúñiga, D., Villacieros-Robineau, N., Salgueiro, E., Alonso-Pérez, F., Rosón, G., Abrantes, F. and Castro, C. G.:
901  Particle fluxes in the NW Iberian coastal upwelling system: Hydrodynamical and biological control, Cont. Shelf
902  Res., 123, 89–98, doi:10.1016/j.csr.2016.04.008, 2016.

903  Zunino, P., Lherminier, P., Mercier, H., Daniault, N., García-Ibáñez, M. I. and Pérez, F. F.: The GEOVIDE cruise
904  in May-June 2014 reveals an intense Meridional Overturning Circulation over a cold and fresh subpolar North
905  Atlantic, Biogeosciences, 14(23), 5323–5342, doi:10.5194/bg-14-5323-2017, 2017.

906

907

908

909

910

911

912

913

914

915

916

917

918

919

920

921

922

923

924

925
926
927
928
929
930

**Table 1:** Summary of the [234]Th export and scavenging fluxes using steady state (SS) and non-steady state (NSS) models. The [234]Th export fluxes using the SS model are calculated at the depths corresponding to the bottom of the primary production zone (PPZ), the equilibrium (Eq) depth and 100 m below Eq (Eq+100); the latter being used to estimate a remineralisation flux of [234]Th (R100). Negative R100 values indicate an increase of the export flux between Eq and Eq+100. Note that the depth was fixed to 100 m at Station 26 because of the lower sampling vertical resolution. Consequently, the export flux at Eq+100 and the R100 were not determined at Station 26.

| Basin | Station | | Export depth m | Th export (SS) dpm m$^{-2}$ d$^{-1}$ | | | Th export (NSS) dpm m$^{-2}$ d$^{-1}$ | | | Th scavenging (SS) dpm m$^{-2}$ d$^{-1}$ | | |
|---|---|---|---|---|---|---|---|---|---|---|---|---|
| Iberian | 1 | PPZ | 155 | 1327 | ± | 137 | | | | | | |
| | | Eq | 90 | 1264 | ± | 104 | 1442 | ± | 80 | 1509 | ± | 189 |
| | | Eq+100 | 190 | 1348 | ± | 199 | | | | | | |
| | | R100 | | -84 | ± | 224 | | | | | | |
| | 13 | PPZ | 82 | 1247 | ± | 99 | | | | | | |
| | | Eq | 110 | 1418 | ± | 111 | 1588 | ± | 86 | 2898 | ± | 285 |
| | | Eq+100 | 210 | 1008 | ± | 187 | | | | | | |
| | | R100 | | 410 | ± | 218 | | | | | | |
| West European | 21 | PPZ | 82 | 1723 | ± | 82 | | | | | | |
| | | Eq | 110 | 1873 | ± | 97 | 2352 | ± | 70 | 3917 | ± | 212 |
| | | Eq+100 | 210 | 1513 | ± | 235 | | | | | | |
| | | R100 | | 360 | ± | 255 | | | | | | |
| | 26 | PPZ | 95 | 1432 | ± | 117 | | | | | | |
| | | Fixed | 100 | 1486 | ± | 117 | 1968 | ± | 98 | 2839 | ± | 220 |
| Icelandic | 32 | PPZ | 75 | 1455 | ± | 92 | | | | | | |
| | | Eq | 130 | 2282 | ± | 119 | 3540 | ± | 113 | 3690 | ± | 199 |
| | | Eq+100 | 230 | 2200 | ± | 227 | | | | | | |
| | | R100 | | 81 | ± | 256 | | | | | | |
| | 38 | PPZ | 70 | 1136 | ± | 80 | | | | | | |
| | | Eq | 80 | 1134 | ± | 95 | 2345 | ± | 115 | 1495 | ± | 160 |
| | | Eq+100 | 180 | 949 | ± | 151 | | | | | | |
| | | R100 | | 185 | ± | 178 | | | | | | |
| Irminger | 44 | PPZ | 37 | 321 | ± | 66 | | | | | | |
| | | Eq | 40 | 321 | ± | 66 | 516 | ± | 90 | 1802 | ± | 71 |
| | | Eq+100 | 140 | 454 | ± | 114 | | | | | | |
| | | R100 | | -132 | ± | 132 | | | | | | |
| | 51 | PPZ | 37 | 495 | ± | 67 | | | | | | |
| | | Eq | 100 | 922 | ± | 103 | 1625 | ± | 108 | 2189 | ± | 260 |
| | | Eq+100 | 200 | 873 | ± | 114 | | | | | | |
| | | R100 | | 49 | ± | 154 | | | | | | |
| Labrador | 64 | PPZ | 83 | 853 | ± | 129 | | | | | | |
| | | Eq | 80 | 855 | ± | 95 | 1423 | ± | 122 | 1142 | ± | 192 |
| | | Eq+100 | 180 | 733 | ± | 200 | | | | | | |
| | | R100 | | 123 | ± | 221 | | | | | | |
| | 69 | PPZ | 35 | 684 | ± | 57 | | | | | | |
| | | Eq | 40 | 758 | ± | 57 | 1068 | ± | 53 | 1257 | ± | 112 |
| | | Eq+100 | 140 | 357 | ± | 148 | | | | | | |
| | | R100 | | 401 | ± | 159 | | | | | | |
| | 77 | PPZ | 55 | 693 | ± | 77 | | | | | | |
| | | Eq | 60 | 696 | ± | 77 | 1169 | ± | 75 | 1529 | ± | 148 |
| | | Eq+100 | 160 | 444 | ± | 146 | | | | | | |
| | | R100 | | 252 | ± | 165 | | | | | | |

931 **Table 2:** Comparison of the steady state POC export fluxes at Eq as determined using the POC:$^{234}$Th ratios in the large
932 (LSF; > 53 μm) and small size fraction (SSF; 1-53 μm).

933

934

| Basin | Station # | LSF POC flux mmol m$^{-2}$ d$^{-1}$ | | | SSF POC flux mmol m$^{-2}$ d$^{-1}$ | | |
|---|---|---|---|---|---|---|---|
| Iberian | 1 | 12 | ± | 22 | 6.9 | ± | 2 |
| | 13 | 2.2 | ± | 0.3 | 3.3 | ± | 0.6 |
| west European | 21 | 4.8 | ± | 0.8 | 6.3 | ± | 1.4 |
| | 26 | 7.9 | ± | 5.0 | 6.1 | ± | 3.7 |
| Icelandic | 32 | 8.3 | ± | 0.5 | 8.8 | ± | 0.5 |
| | 38 | 4.8 | ± | 0.4 | 5.2 | ± | 0.7 |
| Irminger | 44 | 1.4 | ± | 0.5 | 2.4 | ± | 0.5 |
| | 51 | 2.7 | ± | 0.3 | 3.8 | ± | 0.5 |
| Labrador | 64 | 7.8 | ± | 1.5 | 5.5 | ± | 4.9 |
| | 69 | 10 | ± | 1 | 13 | ± | 1 |
| | 77 | 6.1 | ± | 1.5 | 7.5 | ± | 0.9 |

935

936 **Table 3:** POC (particulate organic carbon) to $^{234}$Th ratios (in μmol dpm$^{-1}$) in the LSF, POC export fluxes (in mmol m$^{-2}$ d$^{-1}$), *in-situ* primary production (PP; Fonseca-Batista
937 et al., 2018 and this study) and satellite-derived PP from the Vertically Generalized Production Model (VGPM-PP) integrated over 8 days, 32 days and over the whole
938 season (in mmol m$^{-2}$ d$^{-1}$) and the POC fluxes at Eq+100 m (in mmol m$^{-2}$ d$^{-1}$). Because of the lower vertical sampling resolution at Station 26, no POC export flux was
939 determined at Eq+100. *The sampling to determine the *in-situ* PP at Station 51 occurred 24 h after the sampling of the particulate $^{234}$Th and POC.

| Station | POC:$^{234}$Th at Eq | POC flux at Eq | in-situ PP | 8-days VGPM-PP | 32-days VGPM-PP | seasonal VGPM-PP | POC flux at Eq+100 |
|---|---|---|---|---|---|---|---|
| # | μmol dpm$^{-1}$ | mmol m$^{-2}$ d$^{-1}$ | mmol m$^{-2}$ d$^{-1}$ | mmol m$^{-2}$ d$^{-1}$ | mmol m$^{-2}$ d$^{-1}$ | mmol m$^{-2}$ d$^{-1}$ | mmol m$^{-2}$ d$^{-1}$ |
| 1 | 9 ± 17 | 12 ± 22 | 33 ± 2 | 76 ± 3 | 80 ± 11 | 96 ± 62 | 5.3 ± 23.2 |
| 13 | 1.6 ± 0.2 | 2.2 ± 0.3 | 79 ± 3 | 64 ± 7 | 72 ± 18 | 81 ± 63 | 0.7 ± 0.2 |
| 21 | 2.6 ± 0.4 | 4.8 ± 0.8 | 135 ± 2 | 161 ± 21 | 260 ± 97 | 201 ± 119 | 2.3 ± 0.4 |
| 26 | 5.3 ± 3.3 | 7.9 ± 5.0 | 174 ± 19 | 77 ± 14 | 74 ± 19 | 112 ± 59 | |
| 32 | 3.6 ± 0.1 | 8.3 ± 0.5 | 105 ± 11 | 105 ± 7 | 95 ± 13 | 87 ± 13 | 6.5 ± 0.7 |
| 38 | 4.2 ± 0.1 | 4.8 ± 0.4 | 68 ± 7 | 82 ± 5 | 94 ± 34 | 109 ± 32 | 3.5 ± 0.6 |
| 44 | 4.4 ± 1.3 | 1.4 ± 0.5 | 137 ± 2 | 89 ± 3 | 110 ± 65 | 101 ± 66 | 0.8 ± 0.4 |
| 51 | 2.9 ± 0.01 | 2.7 ± 0.3 | *166 ± 32 | 95 ± 7 | 125 ± 118 | 125 ± 118 | 1.7 ± 0.2 |
| 64 | 9.2 ± 1.1 | 7.8 ± 1.5 | 54 ± 18 | 59 ± 18 | 109 ± 115 | 103 ± 122 | 4.9 ± 1.5 |
| 69 | 14 ± 0.04 | 10 ± 1 | 27 ± 5 | 108 ± 8 | 134 ± 80 | 134 ± 80 | 3.1 ± 1.3 |
| 77 | 8.8 ± 1.9 | 6.1 ± 1.5 | 80 ± 21 | 108 ± 8 | 134 ± 80 | 134 ± 80 | 3.1 ± 1.3 |

940

941
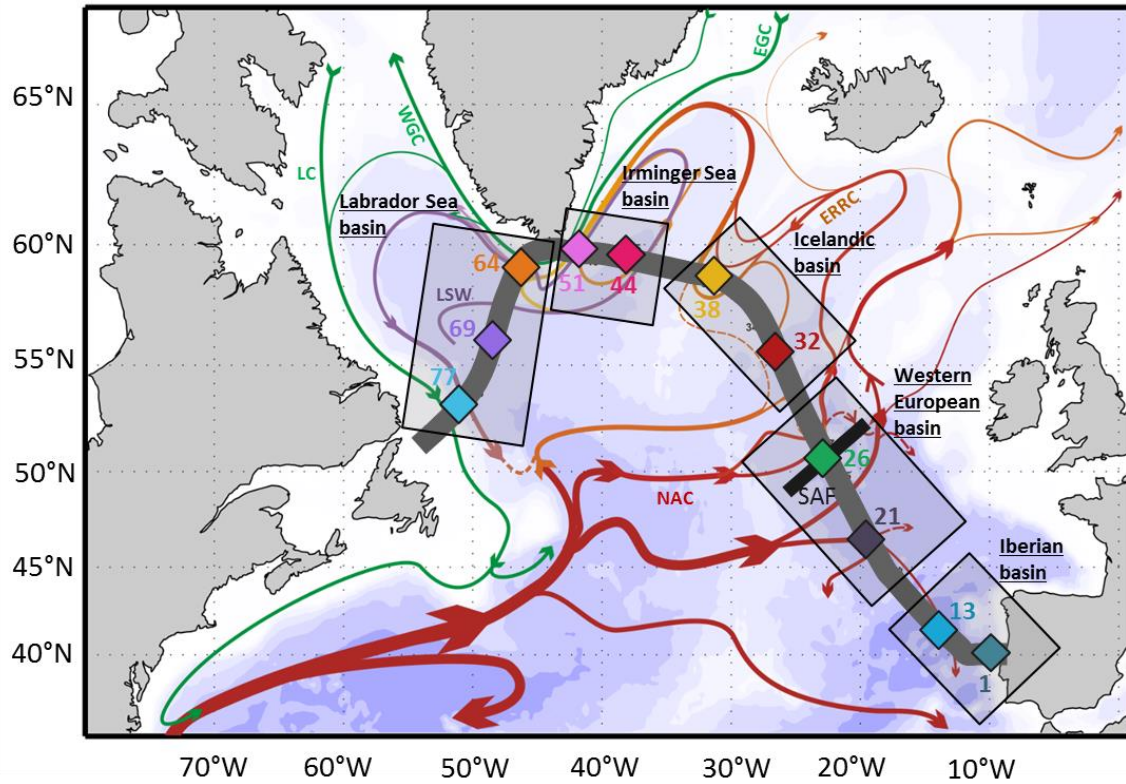
**Figure 1:** Simplified schematic of the surface circulation in the North Atlantic (adapted from Daniault et al., 2016) superimposed with the GEOVIDE cruise track (thick grey line) and stations (colored diamonds). Main surface currents are indicated: East Greenland Current (EGC), West Greenland Current (WGC), Labrador Current (LC), Eastern Reykjanes Ridge Current (ERRC), North Atlantic Current (NAC). The Sub-Arctic Front (SAF) and the Labrador Seawater (LSW) when in surface (i.e. within the Labrador basin) are also represented. The color codes for sampled stations are also used in the following figures.

948
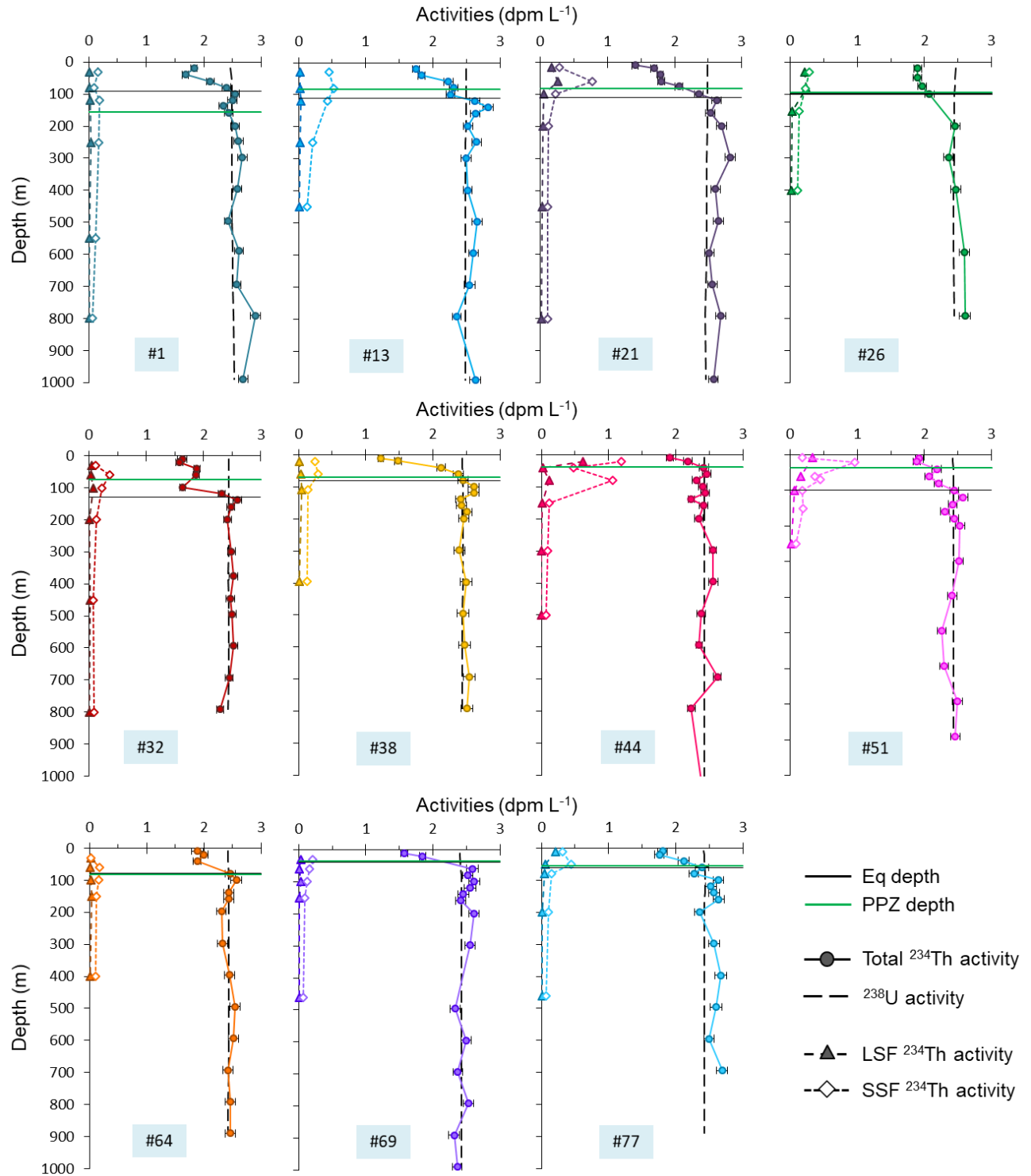
**Figure 2:** Profiles of the total $^{234}$Th (closed circles), total $^{238}$U (black dotted vertical line) and particulate $^{234}$Th activities for the small size fraction (SSF; 1-53 μm; open diamonds) and for the large size fraction (LSF; >53 μm; closed triangles). All activities are expressed in dpm L$^{-1}$. The horizontal black line is the Eq depth (depth where $^{234}$Th returns to equilibrium with $^{238}$U), and the horizontal green line is the depth of the PPZ (primary production zone). Error bars are plotted but may be smaller than the size of the symbols. Note that the Eq depth at Station 26 is fixed at 100 m because of the lower sampling vertical resolution.

POC:²³⁴Th ratios (µmol dpm⁻¹)

955
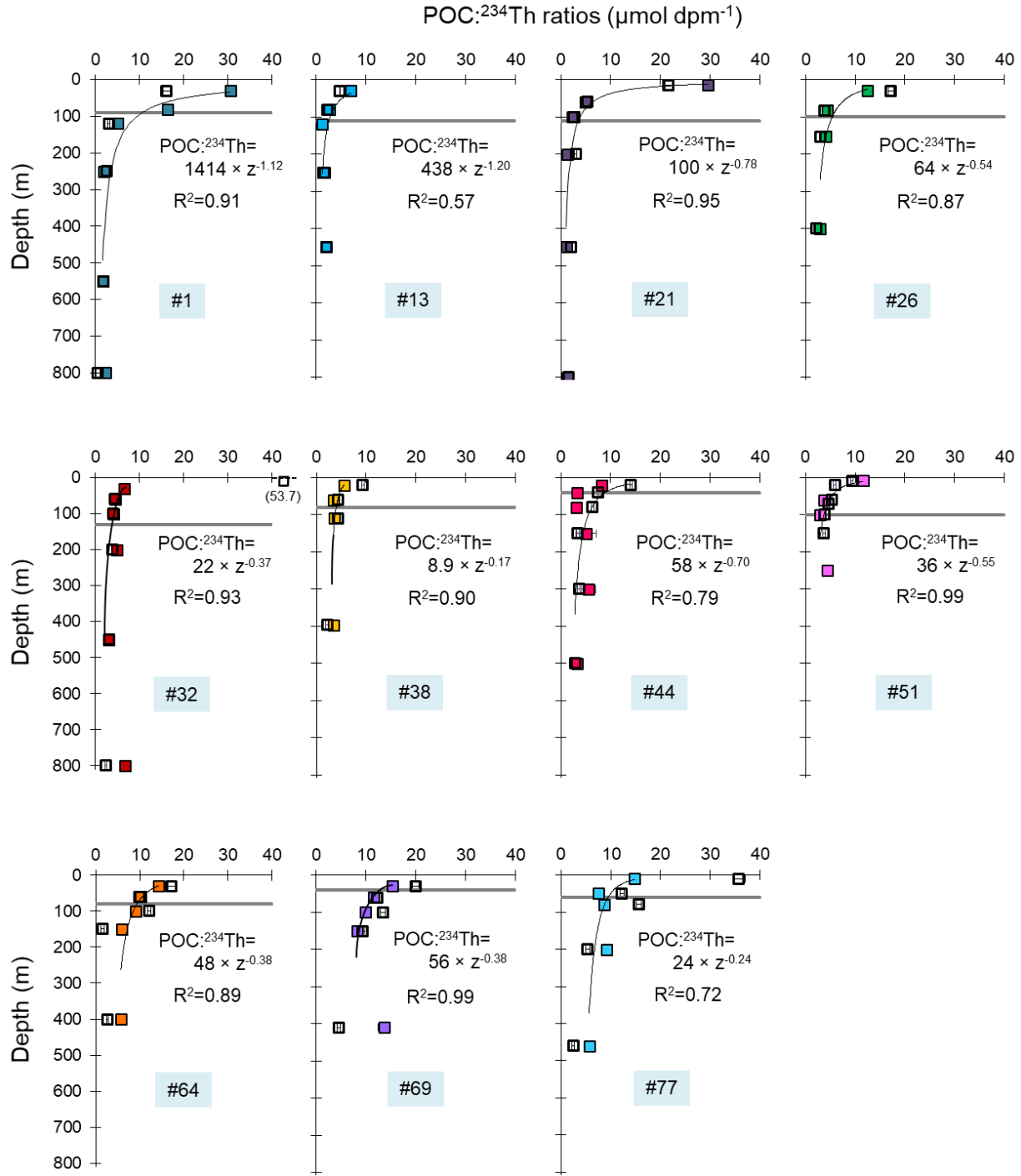
Figure 3: Profiles of the POC:²³⁴Th ratios (µmol dpm⁻¹) in the SSF (open symbols) and LSF (closed symbols). The Eq depth,
where ²³⁴Th is back to equilibrium with ²³⁸U, is indicated with the grey horizontal line. The thin black line represents the
power law fit (POC:²³⁴Th=a×Z⁻ᵇ) of the LSF. The median percentage errors on POC:²³⁴Th ratios are respectively
representing 5 and 6% of the value for the SSF and the LSF. Error bars are plotted but may be smaller than the size of the
symbols.

961
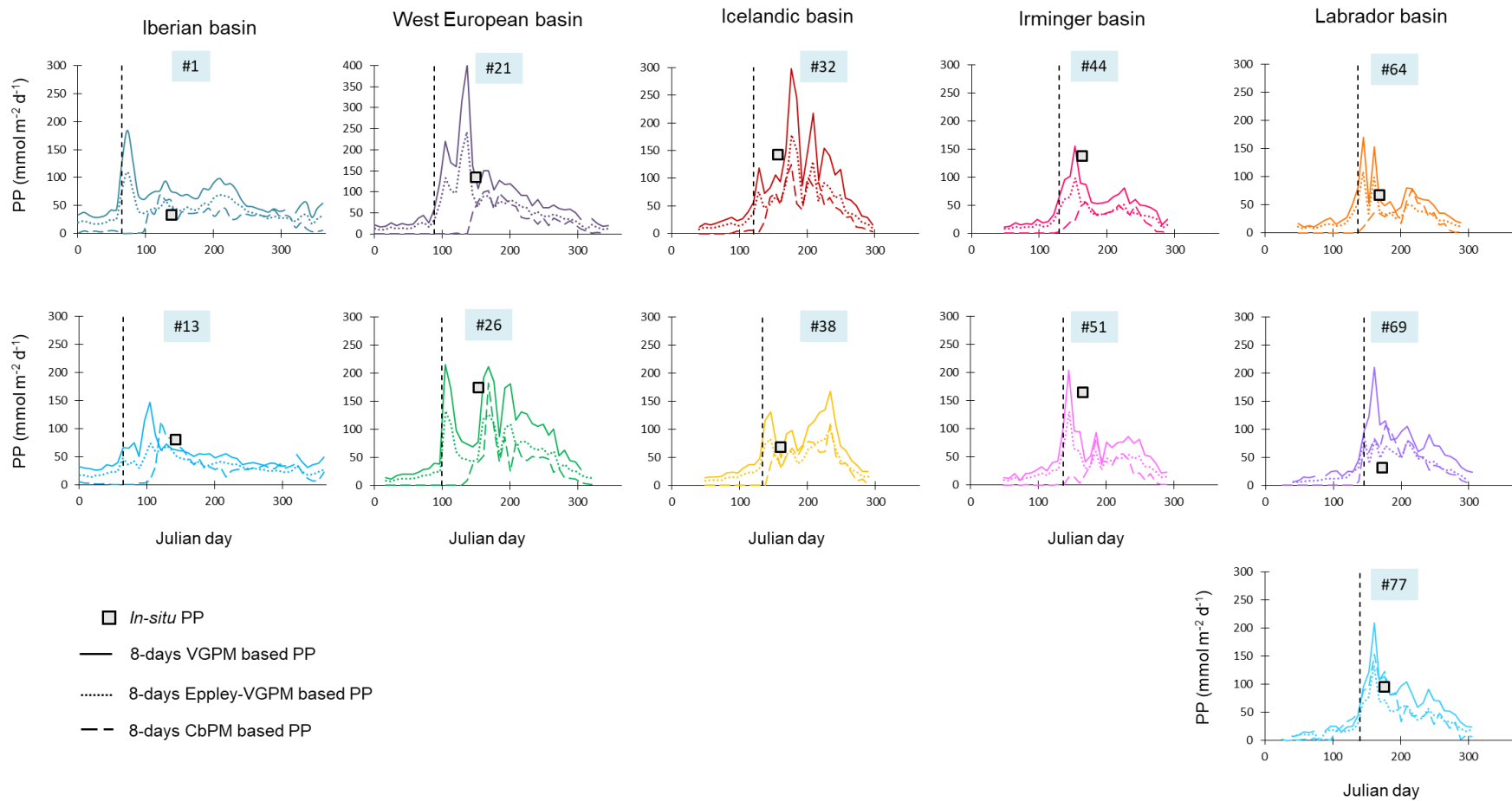
**Figure 4:** *In-situ* (squares) and satellite VGPM-derived (continuous lines), VGPM-Eppley-derived (dotted lines) and CbPM-derived (dashed lines) primary production (PP; in mmol m⁻² d⁻¹) data at the time of our sampling and along the year 2014. The start of the bloom, defined by a PP increase of 30% above the winter value, is indicated with the black vertical dashed line.
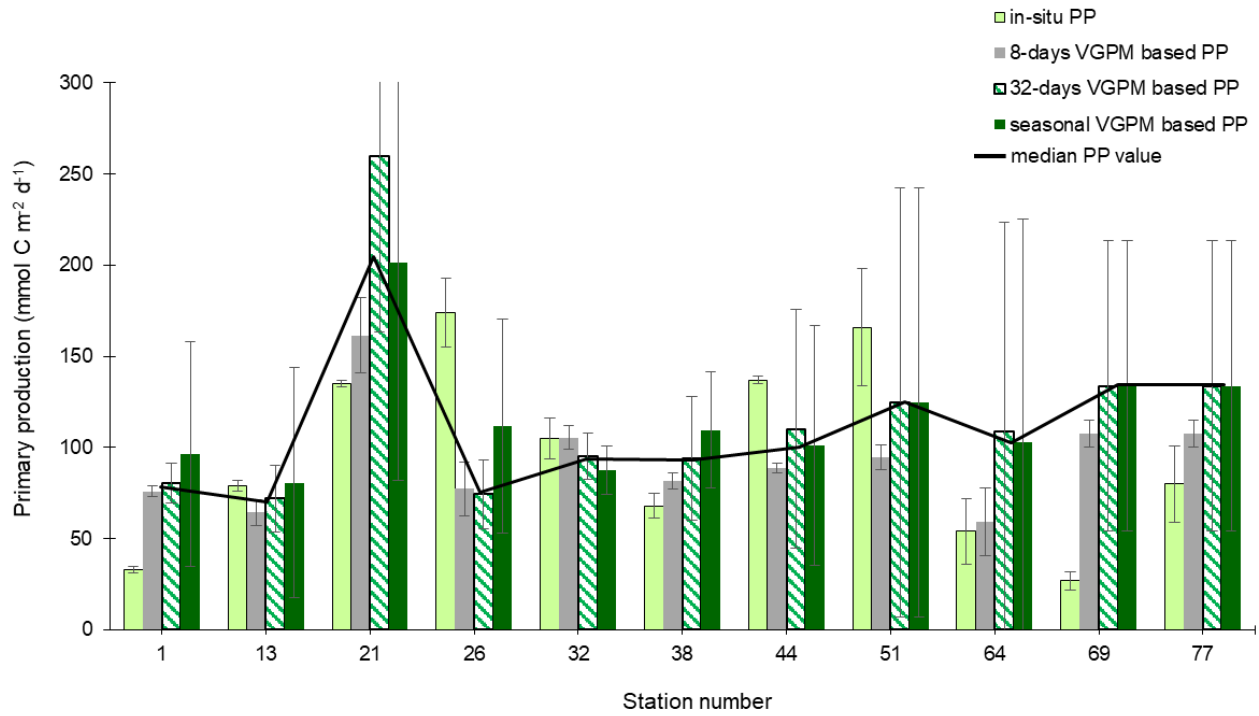
965
966 **Figure 5:** Comparison of *in-situ* and satellite VGPM (8-days, 32-days and seasonal averages) primary productivities (mmol
967 m$^{-2}$ d$^{-1}$) along the GEOVIDE transect. The median of the four values is also indicated (black line).
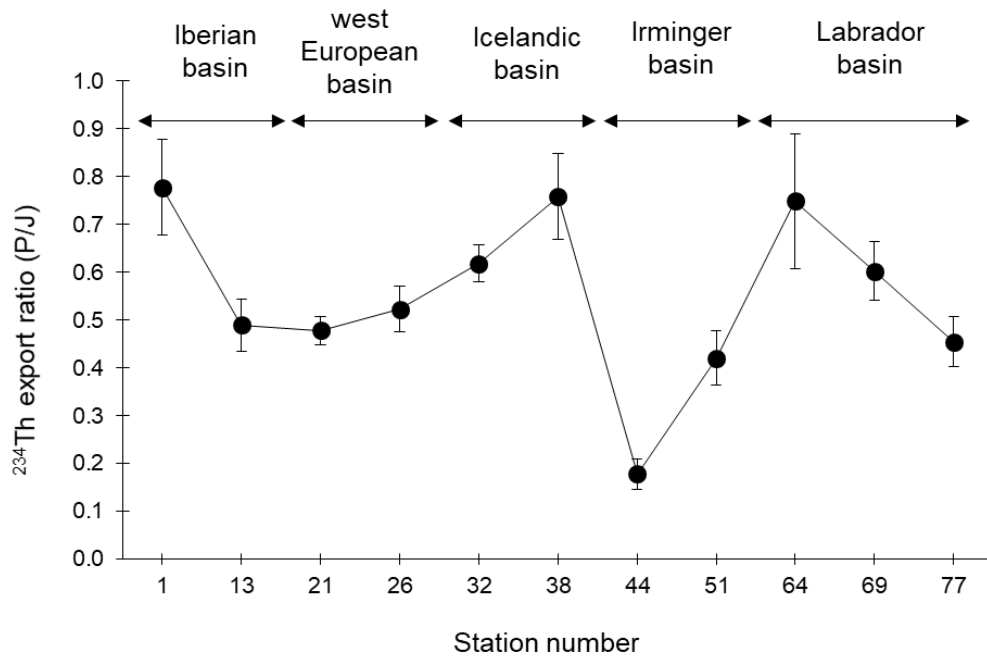
968

969    **Figure 6:** **Variability of the [234]Th export ratio (i.e., the ratio of the [234]Th export flux over the [234]Th scavenged flux; P/J ratio)**
970    **along the GEOVIDE section.**

971
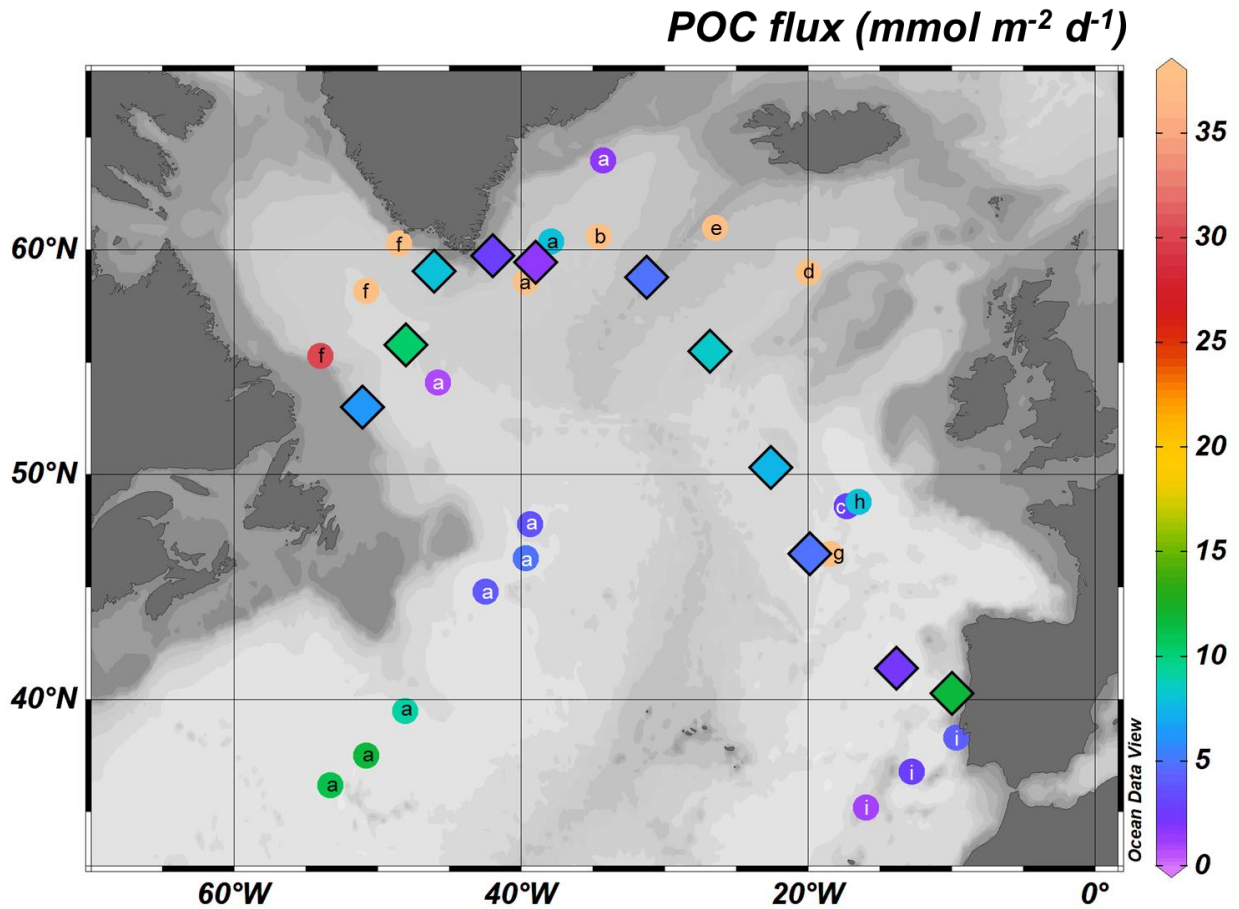
**Figure 7:** Comparison of the POC export fluxes from this study (diamonds with black borders) with other [234]Th-derived estimates of POC exports in the North Atlantic (a: Puigcorbé et al., 2017; b: Ceballos-Romero et al., 2016; c: Thomalla et al., 2008; d: Sanders et al., 2010; e: Martin et al., 2011; f: Moran et al., 2003; g: Buesseler et al., 1992; h: Le Moigne et al., 2013; i: Owens et al., 2015).

972
973
974
975

976

977

978

979

980

981

982

983

984

985

986
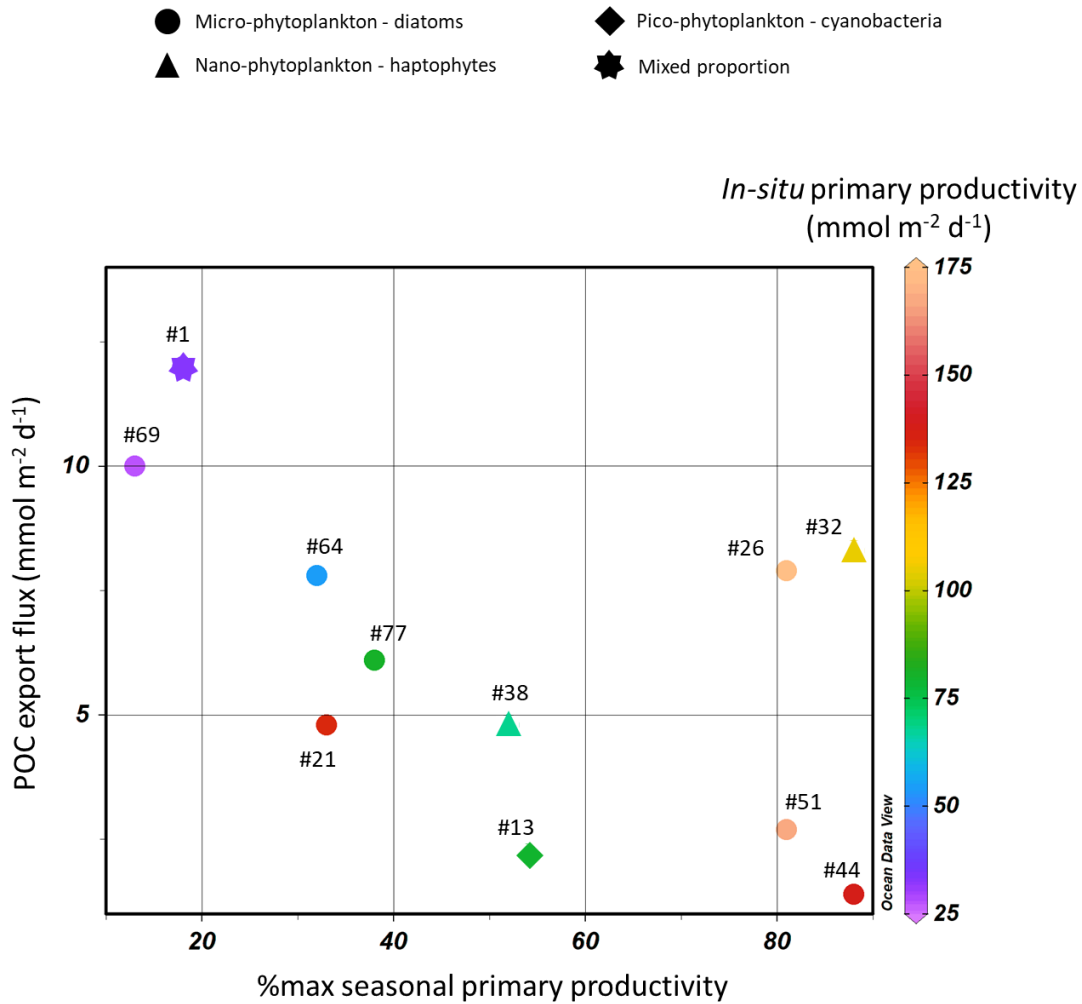
**Figure 8: Percentage of the *in-situ* primary productivity (PP) relative to the maximal VGPM-PP along the season (%max seasonal primary productivity) in function of the POC export fluxes at the Eq depth. The %max seasonal primary productivity illustrates the stage of the bloom (i.e., a %max seasonal primary productivity equalling 100% corresponds to a sampling time at the bloom peak). This relationship is significant when not taking into account the stations sampled between two PP peaks (Stations 26, 32 and 38, see Fig. 4): R2=0.77 and p-value<0.01. The *in-situ* PP measured at sampling time is indicated with the colours in order to indicate the bloom intensity. The dominating phytoplankton community is also indicated, with circles indicating micro-phytoplankton dominance (with a majority of diatoms), triangles nano-phytoplankton dominance (with a majority of haptophytes) and diamonds pico-phytoplankton dominance (with a majority of cyanobacteria). Note that Station 1 is represented by a star because of the mixed proportion of micro-, nano- and pico-phytoplankton.**

987
988
989
990
991
992
993
994
995
996

997

998

999
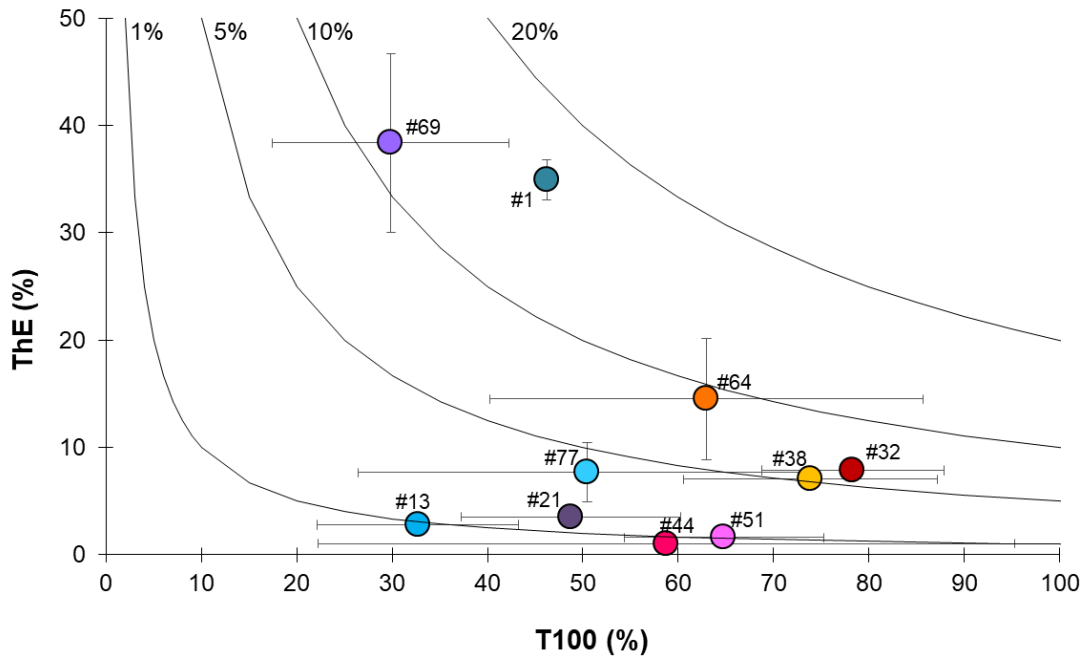
1000

1001 **Figure 9:** **Export efficiency (ThE = Export at Eq /** *in-situ* **PP) versus transfer efficiency (T100 = Export flux at Eq+100 /**
1002 **Export flux at Eq). The black lines represent the modelled 1, 5, 10 and 20% of PP exported to depths > Eq+100 m.**